University of California
Los Angeles

Closed-Loop Subspace Identification of a Quadrotor

A thesis submitted in partial satisfaction
of the requirements for the degree
Master of Science in Engineering

by

Andrew G. Kee

2013

Abstract of the Thesis

Closed-Loop Subspace Identification of a Quadrotor

by

Andrew G. Kee

Master of Science in Engineering

University of California, Los Angeles, 2013

Professor Steve Gibson, Advisor

As quadrotors begin to see extensive use in military and civilian applications, accurate dynamical system models continue to play an important role in platform development, test, and operations. System identification provides a method to estimate dynamical system models from system input and output data. Subspace identification methods exploit the structure of the state space representation of a system to estimate its system matrices up to within a similarity transform. Common subspace identification methods provide reliable results when identifying systems operating in open loop, but produce biased results when identifying systems operating in the presence of feedback (i.e. closed-loop). The Innovation Estimation Method (IEM) provides an approach to eliminating this bias by pre-estimating the unknown innovation sequence before carrying out subspace identification. We describe the identification of an off-the-shelf quadrotor using experimentally gathered closed-loop input-output data through subspace identification with innovation estimation. We present experimental results illustrating the ability of a model identified via IEM to accurately represent system dynamics in the presence of feedback control.

Table of Contents

List of Figures

List of Tables

Nomenclature

F_1, F_2, F_3, F_4	Quadrotor motor forces
r	Vehicle position vector
m	Vehicle mass
g	Gravity
$\mathbb{R}$	Set of all reals
$\mathbb{Z}$	Set of all integers
x	System state vector
A	System matrix
B	Input matrix
C	Output matrix
D	Feedforward matrix
u	System input vector
y	System output vector
e	System innovation vector
n	Number of system states
m	Number of system inputs
l	Number of system outputs
t	Time
v	Process noise vector
w	Measurement noise vector
K	Kalman filter gain
U	Left singular vectors
V	Right singular vectors
k	
f	Future horizon

p	Past horizon
U_p	Block Hankel matrix of past system inputs
U_f	Block Hankel matrix of future system inputs
U_{fi}	i^{th} row of the block Hankel matrix of future system inputs
Y_p	Block Hankel matrix of past system outputs
Y_f	Block Hankel matrix of future system outputs
Y_{fi}	i^{th} row of the block Hankel matrix of future system outputs
X_k	Block Hankel matrix of future system states
X_{k-p}	Block Hankel matrix of past system states
E_p	Block Hankel matrix of past system innovation
E_f	Block Hankel matrix of future system innovation
E_{fi}	i^{th} row of the block Hankel matrix of future system innovation
G_f	Toeplitz matrix of future Markov parameters of stochastic subsystem
G_{fi}	i^{th} row of the Toeplitz matrix of future Markov parameters of stochastic subsystem
H_f	Toeplitz matrix of future Markov parameters of deterministic subsystem
H_{fi}	i^{th} row of the Toeplitz matrix of future Markov parameters of deterministic subsystem
I	Identity matrix
Z_i	Instrumental variable matrix
Z_p	Instrumental variable matrix constructed of past input-output data
u_1, u_2, u_3, u_4	Quadrotor motor commands
p	Vehicle pitch rate
q	Vehicle roll rate

r	Vehicle yaw rate
$\ddot{x}$	Vehicle x-acceleration
$\ddot{y}$	Vehicle y-acceleration
$\ddot{z}$	Vehicle z-acceleration
$\ddot{r}$	Vector of vehicle accelerations
θ	Pitch angle
ϕ	Roll angle
ψ	Yaw angle
$\dot{\Theta}$	Vector of vehicle angular rates
$\hat{\Gamma}_f$	Estimate of extended observability matrix for future horizon
Σ	Diagonal matrix of singular values
σ	Singular value
Γ_k	Extended observability matrix
Γ_{fi}	i^{th} row of the extended observability matrix for future horizon

CHAPTER 1

Introduction

Unmanned Aerial Vehicles (UAVs) have seen explosive growth in the past thirty years, performing a multitude of military and civilian tasks including surveillance, reconnaissance, armed combat operations, search and rescue, forest fire management, and domestic policing [25, 29]. A class of modern UAVs which have recently grown in popularity are quadrotors - Vertical Take Off and Landing (VTOL) vehicles powered by four rotors arranged in a cross or x configuration. The main advantage of the quadrotor lies in its mechanical simplicity. Adjusting the speed of one or more of the vehicle's fixed-pitch rotors provides full attitude control, eliminating the need for the swash plate mechanism found on single rotor helicopters [3, 9]. In spite of its mechanical simplicity, the quadrotor exhibits complex nonlinear dynamics. Because they have only four independent inputs (motor speeds) to control six degrees of freedom (three translational and three rotational), quadrotors are underactuated systems that must be modeled as Multi-Input Multi-Output (MIMO) systems.

Advances in Microelectromechanical Systems (MEMS) and light-weight high-powered lithium polymer batteries have contributed to the recent popularity of quadrotors, making them an attractive choice for research applications in flight dynamics and control, as in [10, 15, 18, 20]. One problem of particular interest is the development of mathematical models representing system dynamics based on experimentally gathered data. System identification provides a mechanism to relate this input-output data to the underlying system dynamics, without as-

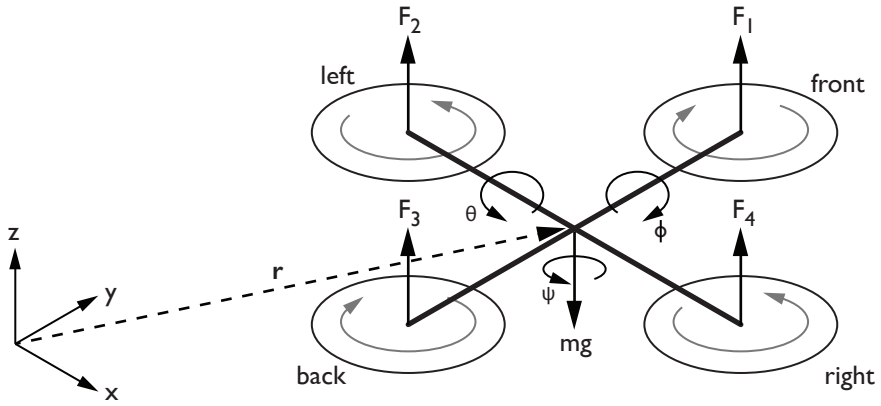

Figure 1.1: A quadrotor arranged in the cross configuration. The position vector of the vehicle's center of mass relative to the inertial reference frame is r. Vehicle pitch is θ, roll is ϕ, and yaw is ψ. Motor forces F_1, F_2, F_3, and F_4 act upwards in the vehicle's body frame and gravity acts downward in the inertial frame.

suming any a priori knowledge of the system. Traditionally, system identification techniques have focused on developing a system model which minimizes prediction error. Identification methods of this form are commonly known as Prediction Error Methods (PEMs). PEMs have seen widespread use in both theoretical and real-world applications, but experience difficulties identifying MIMO systems as noted in [23, 36].

Subspace identification methods (SIMs) have recently grown in popularity and offer an alternative approach to the identification problem. SIMs provide an attractive alternative to PEMs because they identify systems directly in their state space form through the application of non-iterative algorithms. These methods have a foundation in linear algebra and overcome the issues found in PEMs when identifying MIMO systems [13]. While traditional subspace algorithms provide reliable results when identifying systems operating in open loop, modifications must be made to identify systems operating in closed loop to eliminate a bias introduced by feedback control. One such approach, called the Innovation Estimation Method (IEM) eliminates any bias present due to identification using closed-loop data by

pre-estimating the unknown noise sequence before applying a standard subspace identification technique. It is the goal of this research project to apply subspace identification techniques using innovation estimation to a quadrotor using experimentally gathered closed-loop input and output data.

1.1 Related Work

Developing accurate dynamical models of quadrotors plays an important role in their development, test, and continuing operational use. Quadrotors are dynamically unstable and their dynamics are highly nonlinear. Developing system models from first principles is not commonly done due to the complexity of the resulting models and the difficulty of determining numerous unknown system parameters. Several groups have developed simple quadrotor models by directly measuring or estimating system parameters [4, 7, 15, 22, 26], but these models are typically used to select initial controller gains during control system design, and full model simulation results are generally not given.

Using prediction error techniques has proven to be viable approach to identifying quadrotor models from input-output data. In [5], a system model is identified via an AutoRegressive model with external input (ARX) approach using position and attitude data measured by a Cortex 3D camera-based positioning system. NASA's System Identification Programs for Aircraft (SIDPAC) implementation of a least squares PEM is used to individually identify four dynamic modes of a quadcopter (lateral, longitudinal, heave, and yaw) in isolation in [21] with output data measured by a Vicon motion capture system. Both cases showed accurate results when comparing predicted system output with measured system response. Model accuracy is boosted by the use of camera positioning systems to measure system position and attitude, which ensures the output data used for identification is free of some errors present in onboard sensor measurements caused by

accelerometer drift and vehicle vibrations. When camera positioning systems are not available, it is still possible to identify models using measurements taken by onboard accelerometers and gyroscopes. A model developed using prediction error in [17] gave acceptable results when simulating pitch and roll dynamics but did not accurately model yaw dynamics.

Subspace identification techniques have also been shown to produce models which accurately describe quadrotor system dynamics. Motor dynamics were identified using numerical algorithms for subspace state space system identification (N4SID) in [14] and the resulting model was used to simulate vehicle vertical acceleration. In [1], N4SID was used to identify quadrotor roll dynamics from open-loop data collected by fixing all other vehicle degrees of freedom using a test bench setup.

1.2 Motivation and Contributions

As subspace identification techniques continue to evolve, particularly in emerging areas of research including identification of systems in the presence of feedback control, demonstration of empirical results remains important to validate the real world usefulness and application of these theories. The motivation for the work presented here is to show empirical results from the development of dynamical models through subspace identification with innovation estimation. Specifically, we show that a six degree of freedom (6DOF) linear time-invariant (LTI) model of a quadrotor developed using innovation estimation provides an accurate representation of the true dynamical system.

CHAPTER 2

Preliminaries

This document borrows many conepts, techniques, and results from linear algebra and linear systems theory. Because these topics are later presented without discussion, we present an overview them here. This overview is not intended to provide a comprehensive discussion of these topics, rather it serves to introduce the reader to the general topics as they are used in this document.

2.1 Vector and Matrix Notation

We define $\mathbb{R}$ be the set of reals, $\mathbb{R}^n$ the set of n-dimensional real vectors, and $\mathbb{R}^{m\times n}$ the set of real matrices. We denote vectors by lower case letters $\{a,\ b,\ c,\ \dots\}$ and matrices by upper case letters $\{A,\ B,\ C,\ \dots\}$. Transpositions of vectors and matrices are denoted by a^T and A^T, respectively. The inverse of a square matrix A is denoted A^{-1} and its Moore-Penrose psedudoinverse is denoted by $A^\dagger$.

2.2 Linear Systems

2.2.1 Linear Time-Invariant Systems

A discrete time state space representation of a linear dynamical system can be written as

$$x(k+1) = Ax(k) + Bu(k) \tag{2.1a}$$

$$y(k) = Cx(k) + Du(k) \tag{2.1b}$$

where $x(k) \in \mathbb{R}^n$ is a vector of the states of the system, $u(k) \in \mathbb{R}^m$ is a vector of input signals, $y(k) \in \mathbb{R}^l$ is a vector of output signals, and $k \in \mathbb{Z}$ is the time index. A, B, C, and D are the system matrices with dimensions $A \in \mathbb{R}^{n \times n}$, $B \in \mathbb{R}^{n \times m}$, $C \in \mathbb{R}^{l \times n}$, $D \in \mathbb{R}^{l \times m}$.

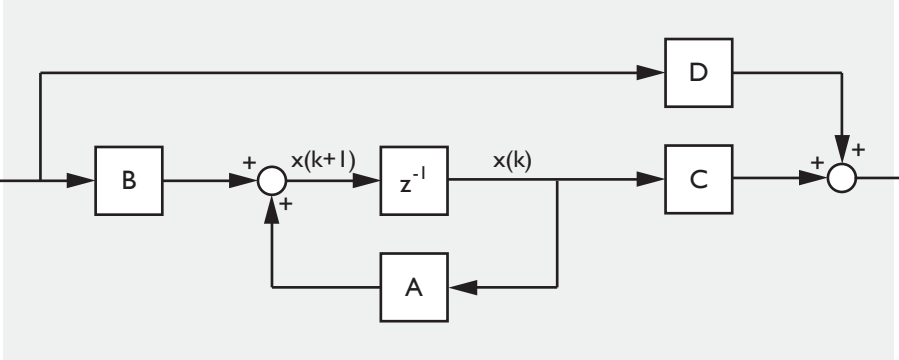

Figure 2.1: A block diagram of the state space representation of a LTI system.

For any state space representation of a system, the state sequence is not unique. That is, there are different state space representations resulting in the same input-output behavior of the system. These differing states can be related by a similarity transform T where T is a real, nonsingular matrix

$$\tilde{x}(k) = T^{-1}x(k)$$

where the tilde in $\tilde{x}$ indicates that it is "similar" to the original state sequence x. The state space representation of the system corresponding to the transformed state $\tilde{x}$ is given by

$$\tilde{x}(k+1) = \tilde{A}\tilde{x}(k) + \tilde{B}u(k)$$

$$y(k) = \tilde{C}\tilde{x}(k) + \tilde{D}u(k)$$

with

$$\tilde{A} = T^{-1}AT, \qquad \tilde{B} = T^{-1}B, \qquad \tilde{C} = CT, \qquad \tilde{D} = D$$

2.2.2 Stability

The LTI system given by A, B, C, D is said to be *stable* if all the eigenvalues of A lie strictly within the unit circle on the complex plane. The system response of a stable LTI system asymptotically converges to a steady state value.

2.2.3 Observability and Controllability

The LTI system given by A, B, C, D or equivalently the pair (A, C) is said to be *observable* if for any finite time $t_1 > 0$, the initial state $x(0) = x_0$ can be uniquely determined from measurements of the input u and output y over the interval $[0, t_1], t_1 > 0$.

The LTI system given by A, B, C, D or equivalently the pair (A, B) is said to be *controllable* if for any final state x_1 there exists an input sequence u_k defined on the interval $[0, t_1], t_1 > 0$ that transfers the state from $x(0) = x_0$ to x_1 in finite time.

LTI systems A, B, C, D in state space form which are both observable and controllable are said to be *minimal*, meaning that the matrix A has the smallest possible dimension.

2.2.4 Combined Deterministic-Stochastic LTI Systems

Section 2.2.1 considered the case of a purely deterministic LTI system; that is, a system operating in a noise-free environment. In practice, this rarely happens so we now consider the case of the combined deterministic-stochastic LTI system operating in the presence of process and measurement noise. We append Eq. 2.1 as follows

$$x(k+1) = Ax(k) + Bu(k) + w(k) \tag{2.3a}$$

$$y(k) = Cx(k) + Du(k) + v(k) \tag{2.3b}$$

where $w(k) \in \mathbb{R}^1$ and $v(k) \in \mathbb{R}^1$ are the process and measurement noises, respectively. As is commonly done, we assume $w(k)$ and $v(k)$ are zero-mean white-noise sequences.

If the system is observable, we can design a Kalman filter to estimate the system state [12]

$$\hat{x}(k+1) = A\hat{x}(k) + Bu(k) + K\big(y(k) - C\hat{x}(k) - Du(k)\big)$$

where K is the Kalman filter gain. If we denote

$$e(k) = y(k) - C\hat{x}(k) - Du(k)$$

to be the innovation sequence, we can rewrite the combined deterministic-stochastic system in Eq. (2.3) in the following equivalent *innovation form*:

$$x(k+1) = Ax(k) + Bu(k) + Ke(k) \tag{2.4a}$$

$$y(k) = Cx(k) + Du(k) + e(k) \tag{2.4b}$$

2.3 Linear Algebra Tools

2.3.1 Fundamental Matrix Subspaces

We require two of the fundamental matrix subspaces: the column space and the row space. The column space of a matrix $A \in \mathbb{R}^{m\times n}$ is the set of all linear combinations of the column vectors of A, sometimes called the range of A. The dimension of the column space is called the rank of A. The row space of a matrix $B \in \mathbb{R}^{m\times n}$ is the set of all linear combinations of the row vectors of B.

2.3.2 Orthogonal Projections

The *orthogonal projection* of the row space of A onto the row space of B is $A\Pi_B$, defined as

$$A\Pi_B = AB^T(BB^T)^{-1}B$$

The projection of the row space of A onto the orthogonal compliment of the row space of B is $A\Pi_B^{\perp}$, defined as

$$A\Pi_B^{\perp} = A\big(I - B^T(BB^T)^{-1}B\big)$$

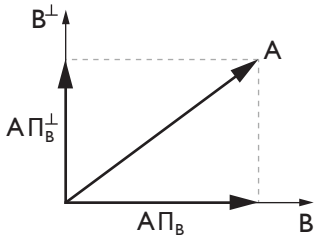

Figure 2.2: Orthogonal projections of A onto B and A onto the orthogonal compliment of B.

Additionally, we define the following properties of orthogonal projections:

$$B\Pi_B = BB^T(BB^T)^{-1}B = B$$

$$B\Pi_B^{\perp} = B\big(I - B^T(BB^T)^{-1}B\big) = B - B = 0$$

When B is large, computing its inverse and thus orthogonal projections onto its subspace is computationally intensive. A more numerically efficient computation of of an orthogonal projection is achieved by LQ decomposition. From the LQ decomposition

$$\begin{bmatrix} B \\ A \end{bmatrix} = \begin{bmatrix} L_{11} & 0 \\ L_{21} & L_{22} \end{bmatrix} \begin{bmatrix} Q_1 \\ Q_2 \end{bmatrix}$$

we have

$$A\Pi_B = L_{21}Q_1$$

$$A\Pi_B^{\perp} = L_{22}Q_2$$

2.3.3 Singular Value Decomposition

Any matrix $A \in \mathbb{R}^{m \times n}$ can be decomposed by a singular value decomposition (SVD) given by

$$A = U \Sigma V^T$$

where $U \in \mathbb{R}^{m \times m}$ and $V \in \mathbb{R}^{n \times n}$ are orthogonal matrices and $\Sigma \in \mathbb{R}^{m \times n}$ is diagonal matrix of the singular values σ_i of A, ordered such that

$$\sigma_1 \geq \sigma_2 \geq \cdots \geq \sigma_r > 0$$

If we partition the matrices in the SVD as

$$A = \left[\begin{array}{c|c} U_1 & U_2 \end{array} \right] \left[\begin{array}{c|c} \Sigma_r & 0 \\ \hline 0 & 0 \end{array} \right] \left[\begin{array}{c} V_1^T \\ \hline V_2^T \end{array} \right]$$

a well known property of the SVD is that the vectors U_1 corresponding to the r non-zero singular values of A span the range of A. That is,

$$\text{range}(U_1) = \text{range}(A)$$

2.3.4 Hankel Matrices

A Hankel matrix is a matrix $A \in \mathbb{R}^{m \times n}$ with constant skew-diagonals:

$$A_{m,n} = \begin{bmatrix} a_1 & a_2 & \cdots & a_n \\ a_2 & a_3 & \cdots & a_{n+1} \\ \vdots & \vdots & \ddots & \vdots \\ a_m & a_{m+1} & \cdots & a_{m+n-1} \end{bmatrix}$$

Hankel matrices can be constructed by setting the i, j^{th} element of A to

$$A_{i,j} = A_{i-1,j+1}$$

If each entry in the matrix is also a matrix, the resulting matrix is called a block Hankel matrix:

2.3.5 Toeplitz Matrices

A Toeplitz matrix is a matrix $A \in \mathbb{R}^{m \times n}$ with constant diagonals.

$$A_{m,n} = \begin{bmatrix} a_1 & a_{-1} & \cdots & a_{-n+1} \\ a_2 & a_1 & \ddots & \vdots \\ \vdots & \ddots & \ddots & a_{-1} \\ a_{m-1} & \cdots & a_2 & a_1 \end{bmatrix}$$

Topelitz matrices can be constructed by setting the i, j^{th} element of A to

$$A_{i,j} = A_{i+1,j+1}$$

CHAPTER 3

Subspace Identification Methods

Subspace identification methods provide an approach to identifing LTI systems in their state space form using input-output data. SIMs provide an attractive alternative to prediction error methods because of their ability to identify MIMO systems and because of their non-iterative solution nature, making them suitable for working with large data sets. In general, the subspace identification problem is: given a set of system input and output data, estimate the system matrices (A, B, C, D) up to within a similarity transform.

Extensive work in both the theory and application of SIMs in the last 20 years has resulted in the development of a number of popular algorithms, including the canonical variate analysis (CVA) method proposed by Larimore [16], the multi-variable output-error state space (MOESP) method proposed by Verhaegen [34], and the numerical algorithms for subspace state space system identification (N4SID) proposed by Van Overschee and De Moor [31]. A unifying theorem subsequently proposed by Van Overschee and De Moor [32] links these algorithms and provides a generalized approach to the subspace identification problem by assigning different weighting matrices for each method.

As described in Van Overschee and De Moor's unifying theorem, all SIMs follow the same general two step procedure. First, estimate the subspace spanned by the columns of the extended observability matrix (Γ_k) from input-output data u_k and y_k. Because the dimension of Γ_k determines the order n of the estimated system, a reduction of the system order is performed before proceeding. Second, the

system matrices are determined, either directly from the extended observability matrix or from the realized state sequence X_k.

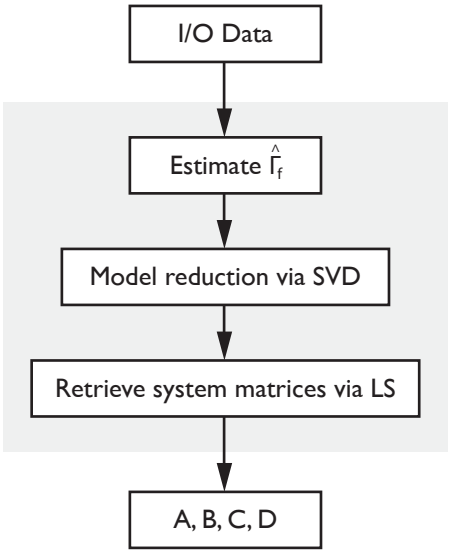

Figure 3.1: Subspace identification approach

3.1 Subspace System Identification

First, we consider the identification of a combined deterministic-stochastic LTI system operating in open loop. We present an overview of the PO-MOESP sub-

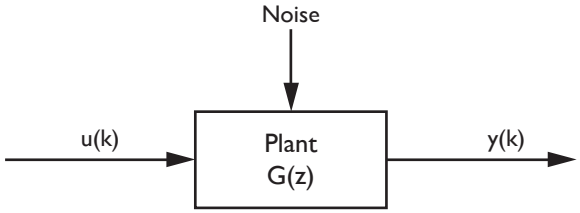

Figure 3.2: A block diagram of an LTI system operating in open loop.

space identification procedure, where "PO" stands for past output, indicating that both past input and output data is used when eliminating the influence of noise on the identified system, further described in Sec. 3.1.2. Before detailing the identification procedure, we introduce the following assumptions:

Assumption 1: The matrix $A - KC$ is stable (i.e. its eigenvalues lie strictly within the unit circle).

Assumption 2: The pair (A, C) is observable and $(A, [B \quad K])$ is controllable.

Assumption 3: The innovation sequence $e(k)$ can be modeled as zero-mean white-noise.

Assumption 4: The input sequence $u(k)$ and innovation sequence $e(k)$ are uncorrelated for all k.

Assumption 5: The input sequence $u(k)$ is persistently exciting.

3.1.1 Extended State Space Model

Recalling the combined deterministic-stochastic LTI system is given in its innovation form as

$$x(k+1) = Ax(k) + Bu(k) + Ke(k) \tag{3.1a}$$

$$y(k) = Cx(k) + Du(k) + e(k) \tag{3.1b}$$

Based on the state space representation, an extended state space model can be formulated as

$$Y_p = \Gamma_p X_{k-p} + H_p U_p + G_p E_p \tag{3.2a}$$

$$Y_f = \Gamma_f X_k + H_f U_f + G_f E_f \tag{3.2b}$$

where p and f denote past and future horizons, respectively. Considering the future horizon given in Eq. 3.2b, the extended observability matrix is

$$\Gamma_f = \begin{bmatrix} C \\ CA \\ \vdots \\ CA^{f-1} \end{bmatrix}$$

and H_f and G_f are Toeplitz matrices of the Markov parameters of the deterministic and stochastic subsystems, respectively:

$$H_f = \begin{bmatrix} D & 0 & 0 & \cdots & 0 \\ CB & D & 0 & \cdots & 0 \\ CAB & CB & D & \cdots & 0 \\ \vdots & \vdots & \vdots & \ddots & \vdots \\ CA^{f-2}B & CA^{f-3}B & CA^{f-4}B & \cdots & D \end{bmatrix}$$

$$G_f = \begin{bmatrix} I & 0 & 0 & \cdots & 0 \\ CK & I & 0 & \cdots & 0 \\ CAK & CK & I & \cdots & 0 \\ \vdots & \vdots & \vdots & \ddots & \vdots \\ CA^{f-2}K & CA^{f-3}K & CA^{f-4}K & \cdots & I \end{bmatrix}$$

We arrange the past and future input sequences into the following block Hankel form with k block rows and N columns:

$$U_p = \begin{bmatrix} u(0) & u(1) & \cdots & u(N-1) \\ u(1) & u(2) & \cdots & u(N) \\ \vdots & \vdots & \ddots & \vdots \\ u(k-1) & u(k) & \cdots & u(k+N-2) \end{bmatrix}$$

$$U_f = \begin{bmatrix} u(k) & u(k+1) & \cdots & u(k+N-1) \\ u(k+1) & u(k+2) & \cdots & u(k+N) \\ \vdots & \vdots & \ddots & \vdots \\ u(2k-1) & u(2k) & \cdots & u(2k+N-2) \end{bmatrix}$$

We construct similar matrices Y_p, Y_f, E_p, and E_f for the output and noise sequences. The state sequences are

$$X_k = \begin{bmatrix} x(k) & x(k+1) & \cdots & x(k+N-1) \end{bmatrix}$$

$$X_{k-p} = \begin{bmatrix} x(k-p) & x(k-p+1) & \cdots & x(k-p+N-1) \end{bmatrix}$$

We will leverage this structure of the extended state space model to identify the unknown system matrices from known input-output data. In particular, we will estimate the column space of the extended observability matrix. Knowledge of this subspace is sufficient to then recover the unknown system matrices.

3.1.2 Estimation of the Extended Observability Matrix

Determination of the system matrices relies on an estimate of the column space of Γ_f. Recalling the extended state space model and again considering only the future horizon, we have

$$Y_f = \Gamma_f X_k + H_f U_f + G_f E_f \tag{3.3}$$

In order to estimate the column space of the extended observability matrix Γ_f in Eq. (3.3), we must eliminate the influence of the input sequence U_f and noise term E_f. The general procedure, as outlined in [23, 35] is as follows: First, we eliminate the influence of the input U_f by multiplying Eq. (3.3) on the right by $\Pi_{U_f}^{\perp}$ where $\Pi_{U_f}^{\perp}$ is an orthogonal projection onto the column space of U_f given by

$$\Pi_{U_f}^{\perp} = I - U_f^T (U_f U_f^T)^{-1} U_f$$

By definition, $U_f \Pi_{U_f}^{\perp} = 0$ so Eq. (3.3) becomes

$$Y_f \Pi_{U_f}^{\perp} = \Gamma_f X_k \Pi_{U_f}^{\perp} + G_f E_f \Pi_{U_f}^{\perp} \tag{3.4}$$

By Assumption 4, the noise term E_f is uncorrelated with the input sequence U_f. That is,

$$E_f \Pi_{U_f}^{\perp} = E_f (I - U_f^T (U_f U_f^T)^{-1} U_f) = E_f$$

so

$$Y_f \Pi_{U_f}^{\perp} = \Gamma_f X_k \Pi_{U_f}^{\perp} + G_f E_f \tag{3.5}$$

Next we eliminate the influence of the noise E_f. In order to remove the influence of the noise on the extended observability matrix, we must introduce an instrumental

variable matrix as described in [35]. We seek a matrix $Z_i \in \mathbb{R}^{2k \times N}$ which exhibits the following properties:

$$\lim_{N\to\infty} \frac{1}{N} E_f Z_i^T = 0 \tag{3.6a}$$

$$\operatorname{rank}\left(\lim_{N\to\infty} \frac{1}{N} X_k \Pi_{U_f}^{\perp} Z_i^T\right) = n \tag{3.6b}$$

Satisfying condition (3.6a) ensures that we can eliminate the noise term E_f by multiplying Eq. (3.5) on the right by Z_i^T and taking the limit for $N \to \infty$:

$$\lim_{N\to\infty} \frac{1}{N} Y_f \Pi_{U_f}^{\perp} Z_i^T = \lim_{N\to\infty} \frac{1}{N} \Gamma_f X_k \Pi_{U_f}^{\perp} Z_i^T \tag{3.7}$$

Satisfying condition (3.6b) ensures multiplication by Z_i does not change the rank of the remaining term on the right hand side of Eq. (3.7) so we have

$$\operatorname{range}\left(\lim_{N\to\infty} \frac{1}{N} Y_f \Pi_{U_f}^{\perp} Z_i^T\right) = \operatorname{range}\left(\Gamma_f\right) \tag{3.8}$$

From Eq. (3.8) we see that an SVD of the matrix $Y_f \Pi_{U_f}^{\perp} Z_i^T$ will provide an estimate of the column space of Γ_f. All that remains is to identify a suitable instrumental variable matrix Z_i. As described in [27, 35], instrumental variable matrices are typically constructed from input-output data. Recalling that we partitioned the input and output data into past and future sets in Section 3.2.1, we will use the future input-output data to identify the system and the past input-output data as the instrumental variable matrix, called Z_p:

$$Z_p = \begin{bmatrix} U_p \\ Y_p \end{bmatrix}$$

Recalling that the noise E_f is uncorrelated with the input U_f for open-loop systems, and enforcing the assumption that E_f is white-noise, we have from [35] that

$$\lim_{N\to\infty} \frac{1}{N} E_f Z_p^T = 0$$

which satisfies condition (3.6a). Jannson showed in [11] that if the input sequence is persistently exciting (Assumption 5), the rank condition (3.6b) on the instrumental variable matrix is satisfied. Taking Z_p as the instrumental variable matrix

and taking the SVD, from Eq. (3.8) we have

$$\hat{\Gamma}_f = US^{1/2} \tag{3.9}$$

3.1.3 Rank Reduction

In the presence of noise, the matrix $Y_f \Pi^{\perp}_{U_f} Z_p^T$ is full rank while the true system order is smaller. We choose the order of the identified system by partitioning the SVD matrices as follows:

$$Y_f \Pi^{\perp}_{U_f} Z_p^T = \begin{bmatrix} U_1 & U_2 \end{bmatrix} \begin{bmatrix} S_1 & 0 \\ 0 & S_2 \end{bmatrix} \begin{bmatrix} V_1^T & V_2^T \end{bmatrix}$$

where the number of singular values n in S_1 is equal to the system order and the remaining submatrices are scaled appropriately. Selecting only the most significant singular values for inclusion in the estimate ensures the true system dynamics are captured while reducing the inclusion of noise. The reduced rank estimate of the extended observability matrix is then

$$\hat{\Gamma}_f = U_1 {S_1}^{1/2} \tag{3.10}$$

3.1.4 Determination of the System Matrices

With an estimate of the column space of Γ_f, we are now able to recover the system matrices. In order to recover the system matrices, we follow the general procedure as outlined in [13]. First, we will exploit the structure of the extended observability matrix to recover the A and C matrices. The matrix C can be read directly from the first block row of $\hat{\Gamma}_f$. In order to recover A, we define the following two modified extended observability matrices:

$$\hat{\overline{\Gamma}}_f = \begin{bmatrix} C \\ \vdots \\ CA^{f-2} \end{bmatrix}, \qquad \hat{\underline{\Gamma}}_f = \begin{bmatrix} CA \\ \vdots \\ CA^{f-1} \end{bmatrix} \tag{3.11}$$

where $\hat{\overline{\Gamma}}_f$ is equal to $\hat{\Gamma}_f$ without the last block row and $\hat{\underline{\Gamma}}_f$ is equal to $\hat{\Gamma}_f$ without the first block row. The structure of the matrices in Eq. (3.11) implies

$$\hat{\overline{\Gamma}}_f A = \hat{\underline{\Gamma}}_f \tag{3.12}$$

which is linear in A and can be solved by least squares.

All that remains is to recover the B and D matrices. We follow the general procedure outlined in [28]. Recalling the extended state space model is given by

$$Y_f = \Gamma_f X_k + H_f U_f + G_f E_f$$

and multiplying on the left by $\hat{\Gamma}_f^{\perp}$ and on the right by ${U_f}^{\dagger}$ we have

$$\hat{\Gamma}_f^{\perp} Y_f {U_f}^{\dagger} = \hat{\Gamma}_f^{\perp} \Gamma_f X_k {U_f}^{\dagger} + \hat{\Gamma}_f^{\perp} H_f U_f {U_f}^{\dagger} + \hat{\Gamma}_f^{\perp} G_f E_f {U_f}^{\dagger} \tag{3.13}$$

where $\hat{\Gamma}_f^{\perp}$ satisfies $\hat{\Gamma}_f^{\perp} \hat{\Gamma}_f = 0$ and $\dagger$ denotes the Moore-Penrose pseudoinverse where $U_f U_f^{\dagger} = 1$. Equation (3.13) simplifies to

$$\hat{\Gamma}_f^{\perp} Y_f {U_f}^{\dagger} = \hat{\Gamma}_f^{\perp} H_f \tag{3.14}$$

Partitioning $\hat{\Gamma}_f^{\perp} Y_f {U_f}^{\dagger}$ into columns with the i^{th} column denoted by $\mathcal{M}_i$ and $\hat{\Gamma}_f^{\perp}$ into rows with the j^{th} row denoted by $\mathcal{L}_j$, Eq. (3.14) is

$$\begin{bmatrix} \mathcal{M}_1 & \mathcal{M}_2 & \cdots & \mathcal{M}_f \end{bmatrix} = \begin{bmatrix} \mathcal{L}_1 \\ \mathcal{L}_2 \\ \vdots \\ \mathcal{L}_f \end{bmatrix} \begin{bmatrix} D & 0 & \cdots & 0 \\ CB & D & \cdots & 0 \\ \vdots & \vdots & \ddots & \vdots \\ CA^{f-2}B & CA^{f-3}B & \cdots & D \end{bmatrix}$$

We can rewrite the above equation as

$$\begin{bmatrix} \mathcal{M}_1 \\ \mathcal{M}_2 \\ \mathcal{M}_3 \\ \vdots \\ \mathcal{M}_f \end{bmatrix} = \begin{bmatrix} \mathcal{L}_1 & \mathcal{L}_2 & \cdots & \mathcal{L}_{f-1} & \mathcal{L}_f \\ \mathcal{L}_2 & \mathcal{L}_3 & \cdots & \mathcal{L}_f & 0 \\ \mathcal{L}_3 & \mathcal{L}_4 & \cdots & 0 & 0 \\ \vdots & \vdots & \ddots & \vdots & \vdots \\ \mathcal{L}_f & 0 & 0 & \cdots & 0 \end{bmatrix} \begin{bmatrix} I & 0 \\ 0 & \hat{\overline{\Gamma}}_f \end{bmatrix} \begin{bmatrix} D \\ B \end{bmatrix} \tag{3.15}$$

which is an overdetermined linear system in B and D. We recover B and D through least squares.

3.1.5 Numerical Efficiencies by LQ Factorization

In the case where N is large, the construction of the matrix $Y_f \Pi_{U_f}^{\perp} Z^T$ in Eq. (3.8) and the subsequent calculation of its SVD are computationally intensive. Verhaegen showed in [33] that from the following LQ decomposition

$$\begin{bmatrix} U_f \\ U_p \\ Y_p \\ Y_f \end{bmatrix} = \begin{bmatrix} L_{11} & 0 & 0 & 0 \\ L_{21} & L_{22} & 0 & 0 \\ L_{31} & L_{32} & L_{33} & 0 \\ L_{41} & L_{42} & L_{43} & L_{44} \end{bmatrix} \begin{bmatrix} Q_1 \\ Q_2 \\ Q_3 \\ Q_4 \end{bmatrix} \tag{3.16}$$

we have

$$\text{range}\left(\lim_{N\to\infty} \frac{1}{\sqrt{N}} \begin{bmatrix} L_{42} & L_{43} \end{bmatrix} \right) = \text{range}\left(\Gamma_f\right) \tag{3.17}$$

This result illustrates the equivalency between Eq. (3.8) and Eq. (3.17), therefore we can estimate the column space of $\hat{\Gamma}_f$ by computing the LQ decomposition in Eq. (3.16), taking the SVD of the matrix $\begin{bmatrix} L_{42} & L_{43} \end{bmatrix}$, and reducing the system order as described previously.

3.2 Closed-Loop Subspace Identification with Innovation Estimation

In many real-world situations, it is either not practical or not possible to collect open-loop input and output data. An unstable system relying on some form of feedback control to operate safely is an example of such a case. It is well known that traditional subspace methods produce biased results in the presence of feedback. This is due to the correlation between the system input and past noise as the controller attempts to eliminate system disturbances [23], violating Assumption 4 introduced in the previous section. As a result, traditional SIMs are not albe to fully decouple the input and noise sequences when estimating the subspace of the extended observability matrix.

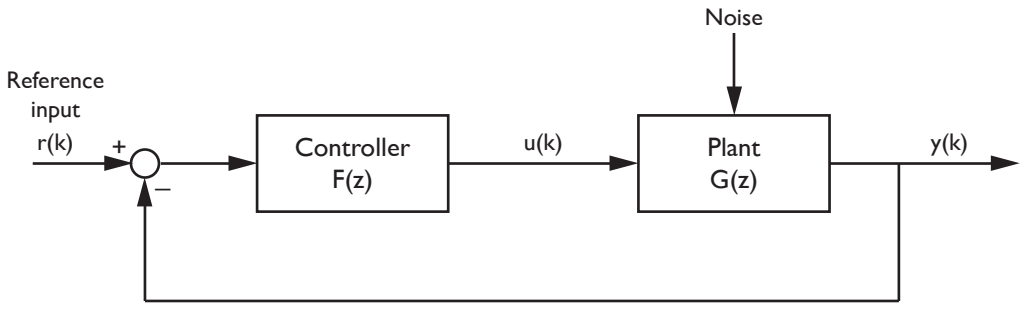

Figure 3.3: A block diagram of an LTI system operating under feedback control.

Recently, several new approaches to identifying closed-loop systems by decoupling inputs from past noise (thus removing any bias) have been proposed. Among these approaches are the innovation estimation method proposed by Qin and Ljung [24] and the Whitening Filter Approach (WFA) proposed by Chiuso and Picci [6]. The IEM pre-estimates the innovation sequence E_f row-wise via a high-order Auto-Regression model with eXogeneous inputs (ARX) algorithm, which is then used to estimate Γ_f from the extended state space model. The WFA partitions a modified version of the extended state space model row-wise and estimates Γ_f through a multi-stage least squares followed by an SVD. It is worth noting that Chiuso and Picci concluded in [6] that while all closed-loop subspace identification algorithms considered produce somewhat biased results in the presence of feedback control, these algorithms are still able to provide significant improvements over traditional SIMs when identifying closed-loop systems.

We now present an overview of the IEM procedure to identify systems operating in closed loop. We assume the following to be true:

Assumption 1: The matrix $A - KC$ is stable (i.e. its eigenvalues lie strictly within the unit circle).

Assumption 2: The pair (A, C) is observable and $(A, [B \quad K])$ is controllable.

Assumption 3: The innovation sequence $e(k)$ is zero-mean white noise.

Assumption 4: The input sequence $u(k)$ is persistently exciting.

3.2.1 Extended State Space Model

We again consider the combined deterministic-stochastic LTI system given in its innovation form as

$$x(k+1) = Ax(k) + Bu(k) + Ke(k) \tag{3.18a}$$

$$y(k) = Cx(k) + Du(k) + e(k) \tag{3.18b}$$

We now assume the system input sequence $u(k)$ is determined through feedback where

$$u(k) = F\big(r(k) - y(k)\big)$$

where $r(k)$ is the reference input. Based on the state space representation, an extended state space model can be formulated as

$$Y_p = \Gamma_p X_{k-p} + H_p U_p + G_p E_p \tag{3.19a}$$

$$Y_f = \Gamma_f X_k + H_f U_f + G_f E_f \tag{3.19b}$$

where p and f denote past and future horizons, respectively. The extended observability matrix is

$$\Gamma_f = \begin{bmatrix} C \\ CA \\ \vdots \\ CA^{f-1} \end{bmatrix}$$

and H_f and G_f are Toeplitz matrices of the Markov parameters of the deterministic and stochastic subsystems, respectively:

$$H_f = \begin{bmatrix} D & 0 & 0 & \cdots & 0 \\ CB & D & 0 & \cdots & 0 \\ CAB & CB & D & \cdots & 0 \\ \vdots & \vdots & \vdots & \ddots & \vdots \\ CA^{f-2}B & CA^{f-3}B & CA^{f-4}B & \cdots & D \end{bmatrix}$$

$$G_f = \begin{bmatrix} I & 0 & 0 & \cdots & 0 \\ CK & I & 0 & \cdots & 0 \\ CAK & CK & I & \cdots & 0 \\ \vdots & \vdots & \vdots & \ddots & \vdots \\ CA^{f-2}K & CA^{f-3}K & CA^{f-4}K & \cdots & I \end{bmatrix}$$

We arrange the input sequence into the following block Hankel form with k block rows and N columns:

$$U_p = \begin{bmatrix} u(0) & u(1) & \cdots & u(N-1) \\ u(1) & u(2) & \cdots & u(N) \\ \vdots & \vdots & \ddots & \vdots \\ u(k-1) & u(k) & \cdots & u(k+N-2) \end{bmatrix}$$

$$U_f = \begin{bmatrix} u(k) & u(k+1) & \cdots & u(k+N-1) \\ u(k+1) & u(k+2) & \cdots & u(k+N) \\ \vdots & \vdots & \ddots & \vdots \\ u(2k-1) & u(2k) & \cdots & u(2k+N-2) \end{bmatrix}$$

We construct similar matrices Y_p, Y_f, E_p, and E_f for the output and noise sequences. The state sequences are

$$X_k = \begin{bmatrix} x(k) & x(k+1) & \cdots & x(k+N-1) \end{bmatrix}$$

$$X_{k-p} = \begin{bmatrix} x(k-p) & x(k-p+1) & \cdots & x(k-p+N-1) \end{bmatrix}$$

3.2.2 Estimation of the Extended Observability Matrix with Innovation Estimation

The extended state space model is

$$Y_f = \Gamma_f X_k + H_f U_f + G_f E_f \tag{3.20}$$

If we partition the extended state space model row-wise, for the i^{th} row we have

$$Y_f = \begin{bmatrix} Y_{f1} \\ Y_{f2} \\ \vdots \\ Y_{ff} \end{bmatrix}, \qquad Y_{fi} = \Gamma_{fi} X_k + H_{fi} U_{fi} + G_{fi} E_{fi} \tag{3.21}$$

where the extended observability matrix is

$$\Gamma_f = \begin{bmatrix} \Gamma_{f1} \\ \Gamma_{f2} \\ \vdots \\ \Gamma_{ff} \end{bmatrix}, \qquad \Gamma_{fi} = CA^{i-1}$$

and the i^{th} rows of H_f and G_f are, respectively

$$H_{fi} = \begin{bmatrix} H_{i-1} & H_{i-2} & \cdots & H_1 & H_0 \end{bmatrix} = \begin{bmatrix} CA^{i-2}B & CA^{i-3}B & \cdots & CB & D \end{bmatrix}$$

$$G_{fi} = \begin{bmatrix} G_{i-1} & G_{i-2} & \cdots & G_1 & G_0 \end{bmatrix} = \begin{bmatrix} CA^{i-2}K & CA^{i-3}K & \cdots & CK & I \end{bmatrix}$$

Additionally, we define

$$H_{fi}^{-} = \begin{bmatrix} H_{i-1} & H_{i-2} & \cdots & H_1 \end{bmatrix} = \begin{bmatrix} CA^{i-2}B & CA^{i-3}B & \cdots & CB \end{bmatrix}$$

$$G_{fi}^{-} = \begin{bmatrix} G_{i-1} & G_{i-2} & \cdots & G_1 \end{bmatrix} = \begin{bmatrix} CA^{i-2}K & CA^{i-3}K & \cdots & CK \end{bmatrix}$$

and derive an equivalent representation of the partitioned state space model as

$$Y_{fi} = \Gamma_{fi} X_k + H_{fi}^{-} U_{i-1} + H_{f1} U_1 + G_{fi}^{-} E_{i-1} + E_{fi} \tag{3.22}$$

By letting $A_K = A - KC$ and $B_K = B - KD$, we are able to derive an expression for the unknown state sequence X_k by iterating Eq. (3.20)

$$X_k = L_p Z_p^T + A_K^p X_{k-p} \tag{3.23}$$

where

$$
\begin{aligned}
X_k &= \begin{bmatrix} x(k) & x(k+1) & \cdots & x(k+N-1) \end{bmatrix} \\
L_p &= \begin{bmatrix} L_p^y & L_p^u \end{bmatrix} \\
L_p^u &= \begin{bmatrix} A_K^{p-1} B_K & A_K^{p-2} B_K & \cdots & B_K \end{bmatrix} \\
L_p^y &= \begin{bmatrix} A_K^{p-1} K & A_K^{p-2} K & \cdots & K \end{bmatrix} \\
Z_p &= \begin{bmatrix} Y_p \\ U_p \end{bmatrix}
\end{aligned}
$$

Substituting Eq. (3.23) into Eq. (3.22) we have

$$Y_{fi} = \Gamma_{fi} L_p Z_p^T + \Gamma_{fi} A_K^p X_{k-p} + H_{fi}^- U_{i-1} + H_{f1} U_1 + G_{fi}^- E_{i-1} + E_{fi} \tag{3.24}$$

Recalling from Assumption 1, we require the eigenvalues of A_K to lie within the unit circle, so for a sufficiently large p, $A_K^p \approx 0$. Additionally, for convenience we assume there is no feedforward term (that is, $D = 0$) then $H_{f1} = 0$ so Eq. (3.24) simplifies to

$$Y_{fi} = \Gamma_{fi} L_p Z_p^T + H_{fi}^- U_{i-1} + G_{fi}^- E_{i-1} + E_{fi} \tag{3.25}$$

or equivalently in matrix form,

$$Y_{fi} = \begin{bmatrix} \Gamma_{fi} L_z & H_{fi}^- & G_{fi}^- \end{bmatrix} \begin{bmatrix} Z_p \\ U_{i-1} \\ E_{i-1} \end{bmatrix} + E_{fi} \tag{3.26}$$

Because the future innovation sequence E_{fi} is uncorrelated with the past innovation sequence E_{i-1}, instrumental variable matrix Z_p, and past output sequence U_{i-1} we see that Eq. (3.25) is formulated in such a way that we can estimate Γ_{fi} row-wise even when the system input and past noise are correlated (i.e. the system is operating with feedback). The only requirement is that future innovation be uncorrelated with past input, which is true for both a pen and closed-loop systems.

In order to estimate the innovation sequence E_f, we consider the first row of the extended state space model by setting $i = 1$ in Eq. (3.25):

$$Y_{f1} = \Gamma_{f1} L_p Z_p^T + E_1 \tag{3.27}$$

We are able to estimate the innovation term E_1 through the following least squares

$$\hat{E}_1 = Y_{f1} - \hat{\Gamma}_{f1} \hat{L}_p Z_p \tag{3.28}$$

with

$$\hat{\Gamma}_{f1} \hat{L}_p = Y_{f1} Z_p^{\dagger} \tag{3.29}$$

In the more general case for $i = 1, 2, \ldots, f$ we have

$$\hat{E}_i = \begin{bmatrix} \hat{E}_{f1} \\ \hat{E}_{f2} \\ \vdots \\ \hat{E}_{f1} \end{bmatrix} = \begin{bmatrix} \hat{E}_{i-1} \\ \hat{E}_{fi} \end{bmatrix} \tag{3.30}$$

thus using Eqs. (3.25) and (3.30) we are able to estimate the innovation sequence recursively using the system input-output data. Once the innovation sequence is known, we are able to estimate the unknown coefficient matrices through least squares as follows:

$$\begin{bmatrix} \hat{\Gamma}_{fi} \hat{L}_p & \hat{H}_{fi}^{-} & \hat{G}_{fi}^{-} \end{bmatrix} = Y_{fi} \begin{bmatrix} Z_p \\ U_{i-1} \\ \hat{E}_{i-1} \end{bmatrix}^{\dagger} \tag{3.31}$$

Computing the least squares estimate of $\hat{\Gamma}_{fi} \hat{L}_z$ row by row using Eq. (3.31), we obtain an estimate of the full matrix $\hat{\Gamma}_f \hat{L}_p$

$$\hat{\Gamma}_f \hat{L}_p = \begin{bmatrix} \hat{\Gamma}_{f1} \hat{L}_p \\ \hat{\Gamma}_{f2} \hat{L}_p \\ \vdots \\ \hat{\Gamma}_{ff} \hat{L}_p \end{bmatrix}$$

from which am estimate of the column space of the extended observability matrix can be obtained via an SVD where

$$\hat{\Gamma}_f = US^{1/2} \tag{3.32}$$

We follow the same procedure outlined in Section 3.1.3 to reduce the rank of the identified system, and recover estimates of the system matrices as in Section 3.1.4

Results from ¡CITE HERE¿ have shown a reduction in bias when identifying systems operating in closed-loop using IEM over traditional SIMs (CVA, N4SID, MOESP). Also, comparisons between the IEM and other closed-loop PEM and subspace identification techniques have shown that under the stated assumptions, estimation differences between the IEM and others are minimal and the IEM provides a consistent system estimate.

CHAPTER 4

Approach

4.1 Quadrotor Platform

Because the design and construction of a quadrotor is beyond the scope of this project, we will use a commercially available vehicle called the Bitcraze Crazyflie [2]. The Crazyflie, shown in Figure 4.1 is a small, low cost, open-source quadrotor kit suitable for indoor flight. It measures 9 cm motor to motor and weighs 19 grams. A 170 mAh lithium-polymer battery powers the vehicle, providing 7 minutes of flight time. An onboard microcontroller is responsible for vehicle stabilization and control and reads sensor measurements from a three-axis accelerometer and a three-axis gyroscope.

Figure 4.1: Bitcraze Crazyflie Quadrotor

Vehicle pitch, roll, yaw, and thrust inputs are set in one of two ways. First, a USB gamepad connected to a computer running the Crazyflie PC client provides a method for direct user control of the vehicle. Second, the PC client exposes a Python API, making it possible to programmatically send the vehicle control set-points. The vehicle receives control inputs and transmits telemetry data wirelessly over a 2.4 GHz radio connection to a USB radio dongle connected to the Crazyflie PC client running on a laptop computer.

The onboard stabilization and control system implements an outer-loop attitude controller and an inner-loop rate controller, as shown in Figure 4.2. Reference pitch and roll commands (θ and ϕ, respectively) are fed to the attitude controller (outputting desired rates) and the reference yaw rate ($\dot{\psi}$) is fed directly to the rate controller. The inner-loop rate control operates at 500 Hz and the outer-loop attitude control operates at 250 Hz.

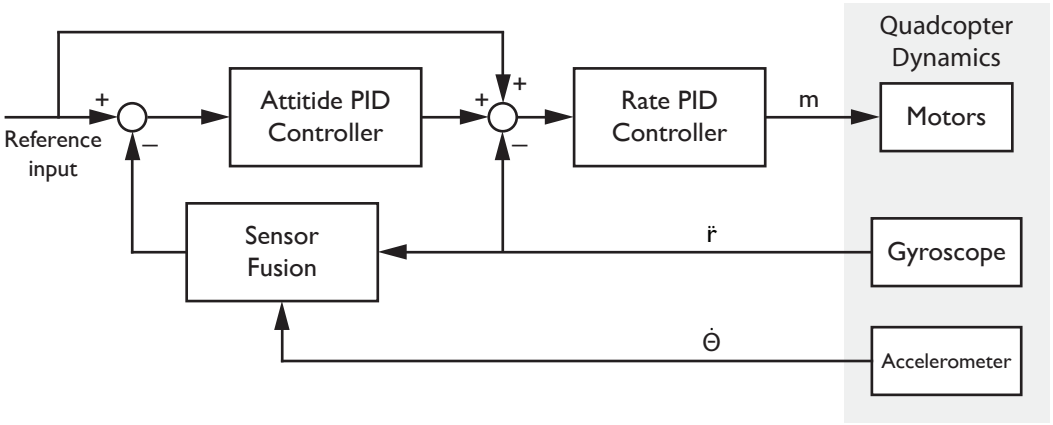

Figure 4.2: Crazyflie stabilization and control system block diagram where $m = \begin{bmatrix} u_1 & u_2 & u_3 & u_4 \end{bmatrix}^T$ is a vector of motor commands, $\ddot{r} = \begin{bmatrix} \ddot{x} & \ddot{y} & \ddot{z} \end{bmatrix}^T$ is a vector of vehicle accelerations, and $\dot{\Theta} = \begin{bmatrix} p & q & r \end{bmatrix}^T$ is a vector of vehicle angular velocities.

4.2 Experimental Collection of Closed-Loop Input-Output Data

In order to develop a robust system model, the input sequence must sufficiently excite all system modes to be identified and the sensor data must be sampled fast enough to avoid aliasing. Because the choices made during experiment design have a direct impact on the identified model, it may be necessary to update aspects of the design if the model is found to be insufficient. In this sense, the development of a system model through system identification may be viewed as an iterative process.

4.2.1 Input Design

The input sequence used to excite the system to be modeled plays an important role in solving the identification problem. Common input sequences used for system identification include impulse signals, doublets, white noise sequences, frequency sweeps, and pseudo-random binary sequences [35]. We considered three major factors when selecting an input sequence:

1. The sequence must be capable of sufficiently exciting all system modes to be identified.

2. The sequence must set the persistence of excitation criteria established in Assumption 4 in Section 3.2.

3. The sequence must be either simple enough to manually execute or formatted in such a way that it is easily transmitted to the vehicle for execution.

Considering the above factors, we chose to use the pseudo-random binary sequence (PRBS) as system input. A PRBS signal, shown in Figure 4.3, is persistently exciting to the order of the period of the signal [37] and is easily transmitted to

the Crazyflie quadcopter by sending input sequences through the Python API.

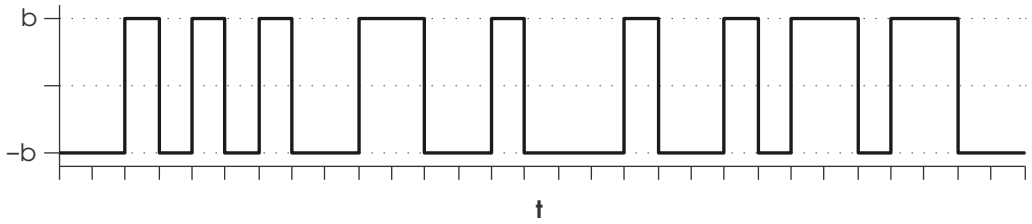

Figure 4.3: A general Pseudo-Random Binary Sequence.

We generated the PRBS signals used for identification by using the MATLAB System Identification Toolbox, specifying the signal period to ensure the persistence of excitation criteria is met. Signals were generated for pitch, roll, and yaw rate. Additional input conditioning was performed to appropriately scale the magnitude of the input signal. Scaling factors were experimentally determined to sufficiently excite the vehicle without rendering it uncontrollable.

Table 4.1: PRBS Scaling Factors

Input	Maximum	Minimum
Pitch	$+25°$	$-25°$
Roll	$+25°$	$-25°$
Yaw Rate	$+50°$/sec	$-50°$/sec

Because the Python API requires system input sequences to be formatted as {pitch, roll, yaw rate, thrust}, we also experimentally determined a thrust input which results in vehicle hover. The general flight test sequence is then: vehicle power on and sensor calibration, take off and hover to an elevation where the vehicle is no longer experiencing ground effect, free flight under PRBS input, landing and vehicle power off. Input signals are sent to the vehicle at 100 Hz. It is worth nothing that the PRBS input does not drive the vehicle directly, instead

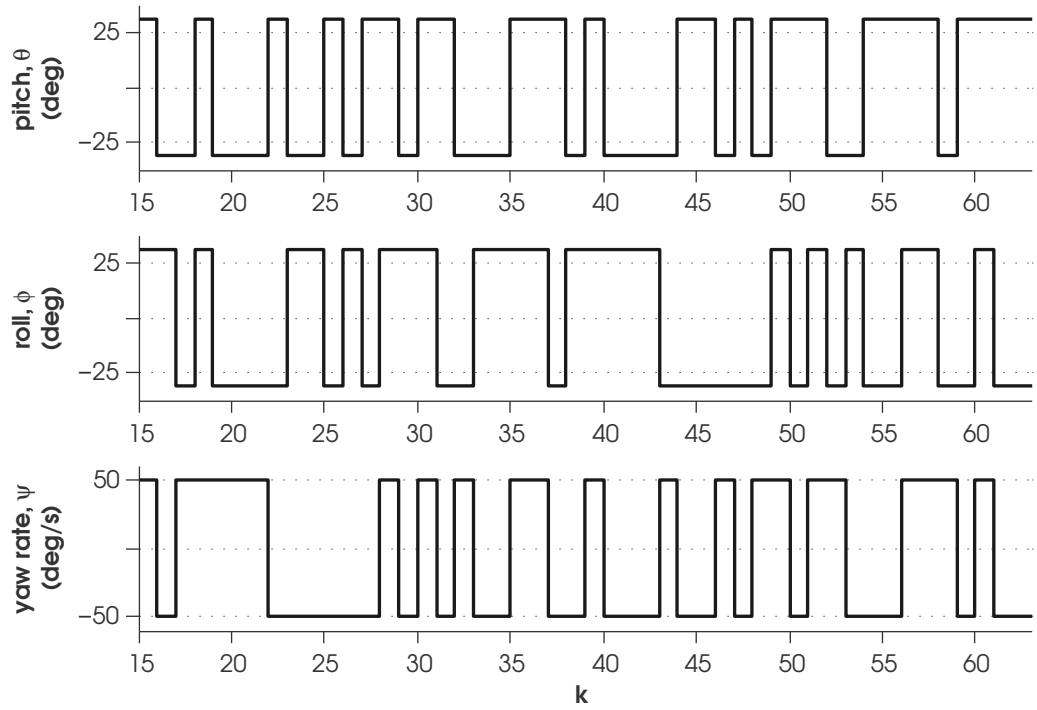

Figure 4.4: A sample PRBS signal used for identification showing scaled inputs for vehicle pitch = ±25°, roll = ±25°, and yaw rate = ±50°/sec.

it acts as a reference input to the controller which in turn commands the vehicle motors. This choice ensures that the vehicle is operating under feedback control and the input-output data gathered is in fact closed-loop data.

4.2.2 Data Collection

System identification requires a rich set of input-output data to identify a suitable model. The Nyquist sampling theorem requires us to sample data at a rate higher than the Nyquist frequency in order to ensure we are able to adequately reconstruct the system input and output signals from logged data [8]. In the case where the full system dynamics are unknown, it is not trivial to exactly identify the Nyquist frequency. Instead, we sample data at a sufficiently fast rate to identify all system dynamics we are interested in modeling.

The PC client logging framework provides a means to log system parameters including motor inputs and onboard sensor measurements. The Crazyflie PC client communicates with the vehicle and receives logged telemetry data using a custom protocol called the Crazy Real Time Protocol (CRTP). CRTP packets are able to carry a maximum of 31 bytes of data and radio bandwidth is user configurable to either 250 kbps, 1 Mbps, or 2 Mbps. The CRTP protocol is configured to give highest priority to user inputs and as a result, may drop non-essential packets if bandwidth is constrained. In order to maximize data logging ability and minimize dropped log packets, we configure the radio to operate at 2 Mbps. Because the log packets are limited to 31 bytes, we split the logged variables into three separate packets as follows: one log packet contains motor input commands for each of the four motors, one log packet contains x, y, and z acceleration measurements, and one log packet contains pitch, roll, and yaw rate measurements from the gyroscope. As a result of the packet size limitation and resulting need to transmit logged variables in three separate packets, the fastest we are able to reliably log data is 50 Hz.

Table 4.2: Logging configuration.

Quantity	Value	Logging Frequency
Motor inputs	Integers of the input command sent to each of the four motors. Values range from 0 to 64000.	50 Hz
Accelerometer measurements	Measurements of x, y, and z accelerations in terms of G's (measured value normalized for gravity)	50 Hz
Gyroscope measurements	Measurements of pitch, roll, and yaw rates in degrees/second.	50 Hz

A suitable test flight location minimizes the introduction of additional disturbances during data collection. In order to avoid the introduction of disturbances from air turbulence and wind gusts, we perform all test flights indoors. Performing all flights on the same day and with a fully charged quadrotor battery further adds to the consistency of the data collected. Test flight length limitations arise from physical room size constraints and battery capacity. The vehicle tends to drift under PRBS inputs, forcing the termination of a test flight any time the vehicle approaches a physical obstacle or wall.

4.3 Data Analysis

Prior to building a model from the sampled data, the raw data is conditioned to provide a more consistent estimate of system dynamics. Following data preprocessing, we perform model identification offline using a finite number of sampled data points.

4.3.1 Data Preprocessing

Before identifying a system model, we must first preprocess the data to make it suitable for use. First we trim the beginning and end of the collected input-output sequences to recover only the data collected when the vehicle is driven by PRBS inputs. This process is achieved by simultaneously plotting all input-output data and visually identifying the beginning and end of the data sequences to retain.

After extracting the usable segment of the collected data, it must be time normalized. SIMs require the input-output data to be uniformly sampled with data points aligning in time. Because the Crazyflie logging framework does not guarantee data is measured and logged simultaneously, we normalize the sampling times by applying a zero-order hold and resampling the data at a uniform rate of 50 Hz.

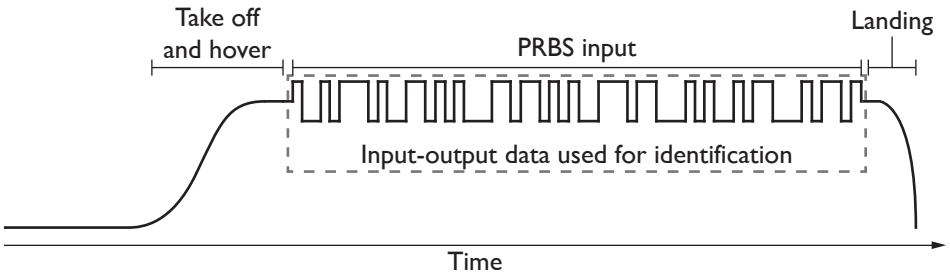

Figure 4.5: Quadrotor test flight profile showing the portion of the test flight data used for system identification.

4.3.2 Model Identification

We identify a model of the unknown system by applying the general procedure outlined in Table 4.3. A MATLAB script processes the data offline and presents results when the algorithm is complete. Before identifying a model, selection of system order and past and future horizons are made. The system order is determined from a plot of the singular values of the extended observability matrix and past and future horizon values are selected as described in Section 4.3.3.

4.3.3 Past and Future Horizon Selection for Innovation Estimation

For SIMs with some form of pre-estimation (such as the pre-estimation of the innovation sequence in the IEM algorithm), past and future time horizons for the estimation step are selected when working with a finite number of data samples. The main purpose of the past horizon is to ensure that $A_K^p \approx 0$ in Eq. (3.24). Care must be taken when selecting the past horizon to avoid over-fitting [30]. The past and future horizons have a significant impact on the resulting identified model's stability and performance and limited guidance exists to help with their precise selection.

4.4 Model Verification

Following identification, we verify the system model by simulating system response to an input sequence and comparing its output with data captured from the physical system using the same input sequence. In order to verify the correctness of the identified model and evaluate its overall performance with respect to the physical system, we simulate model performance with flight test data not used during model identification. Additional flight test data captured while the vehicle undergoes individual excitation of its pitch, roll, and yaw dynamics allows us to evaluate thee model's performance against additional system dynamics.

Table 4.3: Closed-Loop Subspace Identification Algorithm Using Innovation Estimation

1. Recursively estimate the innovation sequence $\hat{E}_i$ row-wise through least squares using

$$Y_{fi} = \Gamma_{fi} L_p Z_p^T + H_{fi}^- U_{i-1} + G_{fi}^- E_{i-1} + E_{fi}$$

2. Estimate the unknown coefficient matrices row-wise through least squares

$$\begin{bmatrix} \hat{\Gamma}_{fi}\hat{L}_p & \hat{H}_{fi}^- & \hat{G}_{fi}^- \end{bmatrix} = Y_{fi} \begin{bmatrix} Z_p \\ U_{i-1} \\ \hat{E}_{i-1} \end{bmatrix}^\dagger$$

and form the matrix $\hat{\Gamma}_f \hat{L}_p$

3. Estimate the column space of the extended observability matrix from an SVD of $\hat{\Gamma}_f \hat{L}_p$ and appropriately reduce the model order where

$$\hat{\Gamma}_f = U_1 S_1^{1/2}$$

4. Recover an estimate of C directly from the first block row of $\hat{\Gamma}_f$ and A by solving the least squares problem

$$\hat{\overline{\Gamma}}_f A = \hat{\underline{\Gamma}}_f$$

5. Recover estimates of B and D by solving the least squares problem

$$\begin{bmatrix} \mathcal{M}_1 \\ \mathcal{M}_2 \\ \mathcal{M}_3 \\ \vdots \\ \mathcal{M}_f \end{bmatrix} = \begin{bmatrix} \mathcal{L}_1 & \mathcal{L}_2 & \cdots & \mathcal{L}_{f-1} & \mathcal{L}_f \\ \mathcal{L}_2 & \mathcal{L}_3 & \cdots & \mathcal{L}_f & 0 \\ \mathcal{L}_3 & \mathcal{L}_4 & \cdots & 0 & 0 \\ \vdots & \vdots & \ddots & \vdots & \vdots \\ \mathcal{L}_f & 0 & 0 & \cdots & 0 \end{bmatrix} \begin{bmatrix} I & 0 \\ 0 & \hat{\overline{\Gamma}}_f \end{bmatrix} \begin{bmatrix} D \\ B \end{bmatrix}$$

CHAPTER 5

Closed-Loop Subspace Identification of a Quadrotor

5.1 Identification Results

Using closed-loop input-output data captured from test flights of a quadrotor operating under PRBS inputs, we developed an LTI system model using subspace identification techniques with innovation estimation following the procedure outlined in Chapter 4.

5.1.1 Experimental Data Used for Identification

We conducted many test flights and ultimately identified 18 data sequences of high enough quality to use for model identification and verification. Of these sequences, nine were collected with the vehicle operating under PRBS inputs and nine were collected with the vehicle operating under individual DOF excitation inputs (three each for pitch, roll, and yaw). While we considered concatenating multiple data sequences together into a longer single input-output sequence, models identified with an individual sequence proved to adequately capture desired system dynamics.

5.1.2 Model Order Selection

System order selection occurs as a part of the model identification procedure. A plot of the singular values of the extended observability matrix, shown in Figure 5.1 is intended to provide a visual means to select the best system order. From the figure, we see a significant drop in the magnitude of the singular values after the second, but selecting a system order of two did not adequately model the system dynamics. As a result, we tested a number of models with orders ranging from 3 to 12 and ultimately selected an 8th order model because it consistently produced reliable results from multiple PRBS data sets.

5.1.3 Past and Future Horizon for Innovation Estimation

Estimation of the innovation sequence requires the definition of past and future estimation horizons. We experimentally determined past and future horizon values by identifying a number of system models by varying the past and future horizons, first in coarse increments and later in finer increments. By evaluating

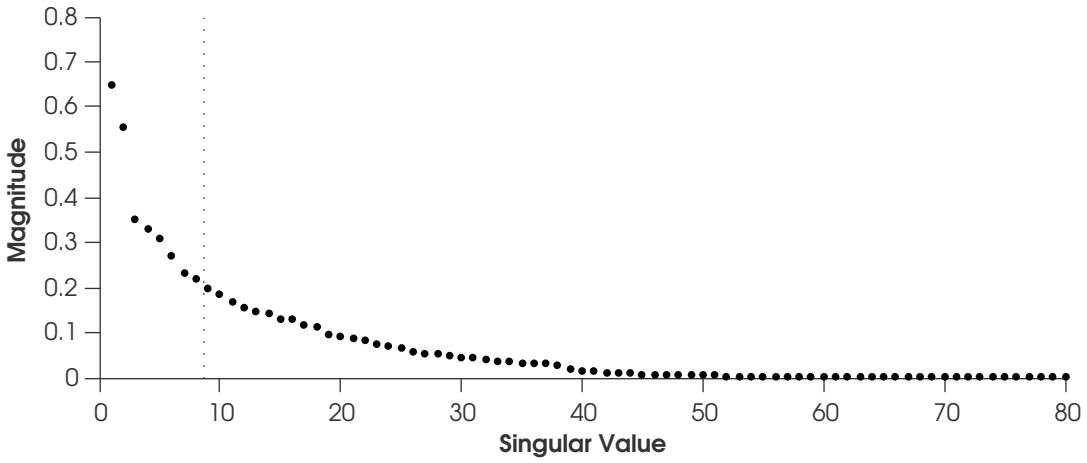

Figure 5.1: A plot of the singular values of the extended observability matrix, used to determine the model order. The vertical dotted line shows the partitioning location between system response and noise in the final eighth order model.

the performance of a set of models identified over a range of coarsely spaced horizons, we were able to narrow the time horizon window and evaluate a smaller set of models identified over a range of finely spaced horizons, eventually settling on the best model. For the final system model, we used a past estimation horizon of 60 and a future estimation horizon of 17.

By plotting the poles of all evaluated models (Figure 5.2), we see the most common pole locations. The poles of the final system model, plotted in Figure 5.3 show the model is stable and only one pole has an oscillatory response (the pole is located in the left half of the real plane). This is in contrast to the full set of models, which most commonly have three poles exhibiting an oscillatory response. The single oscillatory pole in the final system model is also faster than each of the three poles common to the set of all models, which increases the overall responsiveness of the final model.

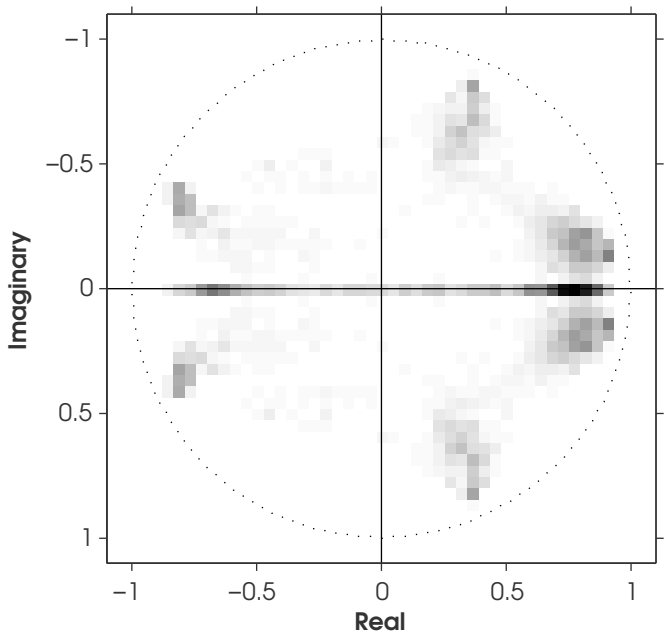

Figure 5.2: Pole distribution of 8th order models generated for 756 combinations of past and future horizons. Darker shading indicates higher pole concentrations.

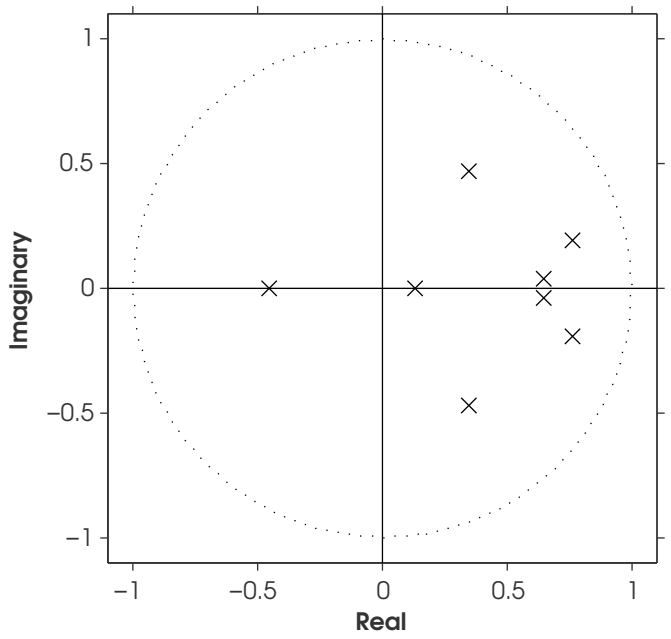

Figure 5.3: Poles of final 8th order model.

5.1.4 Identified 6DOF Quadcopter Model

The final 8th order quadrotor LTI model identified using innovation estimation, given in its state space form is

$$x(k+1) = Ax(k) + Bu(k)$$

$$y(k) = Cx(k) + Du(k)$$

where system input $u = \begin{bmatrix} u_1 & u_2 & u_3 & u_4 \end{bmatrix}^T$ is a vector of motor commands and system output $y = \begin{bmatrix} \ddot{x} & \ddot{y} & \ddot{z} & p & q & r \end{bmatrix}^T$ is a vector of accelerometer and gyroscope measurements. The system matrices of the model appear fully in Table 5.1.

Table 5.1: Identified System Matrices, 8th order LTI Quadrotor Model

$$A = \begin{bmatrix} 0.8521 & -0.0304 & -0.2107 & 0.3639 & 0.0859 & -0.2501 & 0.0172 & -0.0448 \\ -0.0794 & 0.7874 & 0.1238 & 0.2699 & 0.4075 & 0.0408 & -0.3177 & -0.0088 \\ 0.1025 & -0.0053 & 0.5120 & -0.4573 & 0.3561 & -0.5139 & 0.0986 & -0.1669 \\ -0.0379 & 0.0325 & -0.5483 & -0.3013 & 0.4049 & -0.0075 & 0.1634 & 0.3805 \\ 0.0042 & -0.0926 & 0.0224 & 0.1017 & 0.5170 & 0.3392 & 0.5775 & -0.2288 \\ 0.1567 & -0.0832 & 0.5616 & 0.2255 & -0.0186 & 0.3945 & 0.2078 & 0.4095 \\ 0.0077 & 0.0579 & 0.0469 & 0.0398 & -0.0686 & -0.2426 & -0.0026 & 0.2523 \\ -0.0622 & 0.0535 & -0.0811 & 0.0428 & 0.1020 & -0.0254 & 0.0795 & 0.4353 \end{bmatrix}$$

$$B = \begin{bmatrix} -0.0025 & -0.0037 & -0.0112 & -0.0017 \\ 0.0022 & 0.0027 & 0.0039 & 0.0045 \\ -0.0038 & -0.0018 & 0.0101 & -0.0024 \\ 0.0098 & 0.0090 & -0.0020 & 0.0037 \\ -0.0011 & 0.0063 & -0.0035 & 0.0027 \\ 0.0077 & 0.0107 & 0.0038 & 0.0054 \\ -0.0009 & -0.0085 & -0.0032 & -0.0058 \\ -0.0013 & -0.0042 & -0.0072 & -0.0047 \end{bmatrix}$$

$$C = \begin{bmatrix} -0.0001 & 0 & -0.0001 & 0.0001 & -0.0001 & 0.0002 & 0.0003 & -0.0003 \\ 0 & 0 & 0.0001 & -0.0001 & 0.0002 & -0.0001 & -0.0002 & 0.0003 \\ 0.0001 & -0.0001 & 0 & 0 & -0.0002 & 0.0003 & 0.0000 & -0.0004 \\ -0.0252 & -0.5396 & 0.0367 & 0.0661 & 0.4731 & 0.1647 & -0.6491 & 0.0088 \\ -0.4569 & -0.2298 & -0.0069 & 0.6147 & 0.1088 & -0.5000 & 0.1831 & 0.0206 \\ -0.0116 & 0.0591 & 0.0035 & 0.0091 & 0.0085 & -0.0450 & 0.0297 & -0.0022 \end{bmatrix}$$

$$D = \begin{bmatrix} 0 & 0 & 0 & 0 \\ 0 & 0 & 0 & 0 \\ 0 & 0 & 0 & 0 \\ 0 & 0 & 0 & 0 \\ 0 & 0 & 0 & 0 \\ 0 & 0 & 0 & 0 \end{bmatrix}$$

5.2 Time Domain Model Validation

Comparing system response predicted by the identified model with measured system response originating from the same input sequence provides a straightforward way to validate the identified model in the time domain. We compared the identified model's time domain response with the measured response of the physical system using four different input sequences: PRBS input, pure pitch input, pure roll input, and pure yaw input.

Because the IEM deals with the coupling between system input and past noise present in a closed-loop system by pre-estimating the noise sequence from the input-output data used for identification, some real system dynamics are inevitably "estimated out" of the model during this procedure. This is evident in the fact that some of the faster system modes are not perfectly represented.

By evaluating the identified model's ability to represent the decoupled dynamics of the physical system, we are able to draw conclusions about the ability of a PRBS input sequence to identify individual dynamical modes of a system. During the pure pitch, roll, and yaw input sequences, the non-excited degrees of freedom were not fixed and thus the vehicle was free to move in all six degrees of freedom.

5.2.1 Evaluation of Full 6DOF LTI Model Dynamics

Figure 5.4 shows the comparison of system response between the identified model and the physical system. In general, the identified model provides a satisfactory estimate of the physical system dynamics. The pitch and roll rates are accurately predicted and the magnitudes of the x, y, and z accelerations are correctly predicted.

While the system acceleration predictions are accurate with respect to the magnitude of acceleration, it is not surprising that the predictions do not more closely follow the measured response. This is due to the fact that the accelerometers are

very susceptible to measuring vehicle vibrations caused by slightly unbalanced motors and propellers. Because these vibrations occur at a much higher frequency than the Nyquist frequency, they are not captured by the identified model and thus not reflected in the system response.

Inspecting the yaw rate response, we see that the model does not accurately capture the yaw dynamics of the physical system. We observed this deficiency in all verification tests when comparing simulated model response with the measured response of the physical system. We hypothesize that this failure to successfully identify the yaw dynamics is due to the way a quadrotor's yaw mode is excited. While the pitch and roll modes of a quadrotor are excited by changing the rotor speed of only two opposing rotors, excitation of the yaw mode requires speed changes to all four rotors. It is possible that a higher order system model would capture these dynamics, although we tested models up to 12th order without success. This problem is not isolated; others including [17] and [19] have experienced similar difficulties identifying yaw dynamics in rotorcraft.

5.2.2 Evaluation of LTI Model Pitch Dynamics

Figure 5.5 shows the comparison of system response between the identified model and the physical system excited by pure pitch inputs. The simulated pitch rate aligns with the measured value showing that the model accurately represents isolated pitch dynamics of the system.

5.2.3 Evaluation of LTI Model Roll Dynamics

Figure 5.6 shows the comparison of system response between the identified model and the physical system excited by pure roll inputs. The simulated roll rate generally tracks the measured value. In several places, the measured roll rate is clipped while the predicted value is not clipped (in particular between 1.5 and 2

seconds). This is likely due to nonlinearities in the physical system not captured by the linear model.

5.2.4 Evaluation of LTI Model Yaw Dynamics

Figure 5.7 shows the comparison of system response between the identified model and the physical system excited by pure yaw inputs. The identified model does not accurately capture the isolated yaw dynamics of the physical system. This is expected, as the model also failed to adequately represent the yaw dynamics of the full 6DOF system operating under PRBS input. Inspection of the pitch and roll rate responses in Figure 5.7 reveals a coupling between yaw input and simulated pitch and roll rate. Both yaw inputs beginning at 1.7 seconds and 2.2 seconds result in responses in simulated pitch and roll rates. This effect is not seen in the physical system. The yaw dynamics are not completely missed however. From Figure we see that after 2 seconds, the simulated response somewhat tracks the measured output for small angle changes.

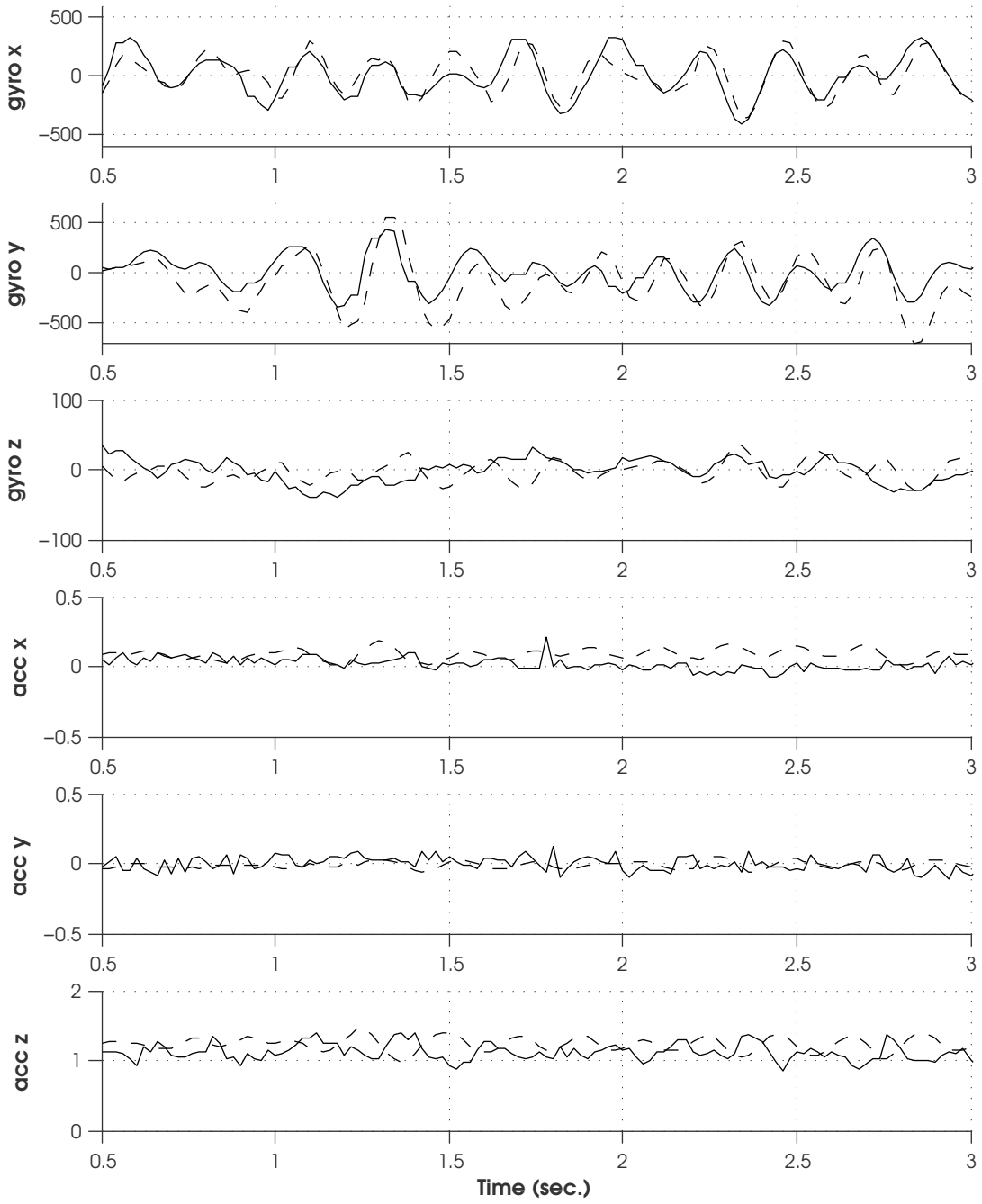

Figure 5.4: Simulated response (dashed) of identified 8th order LTI system model compared with measured system response (solid). Both systems were stimulated with an identical PRBS input sequence.

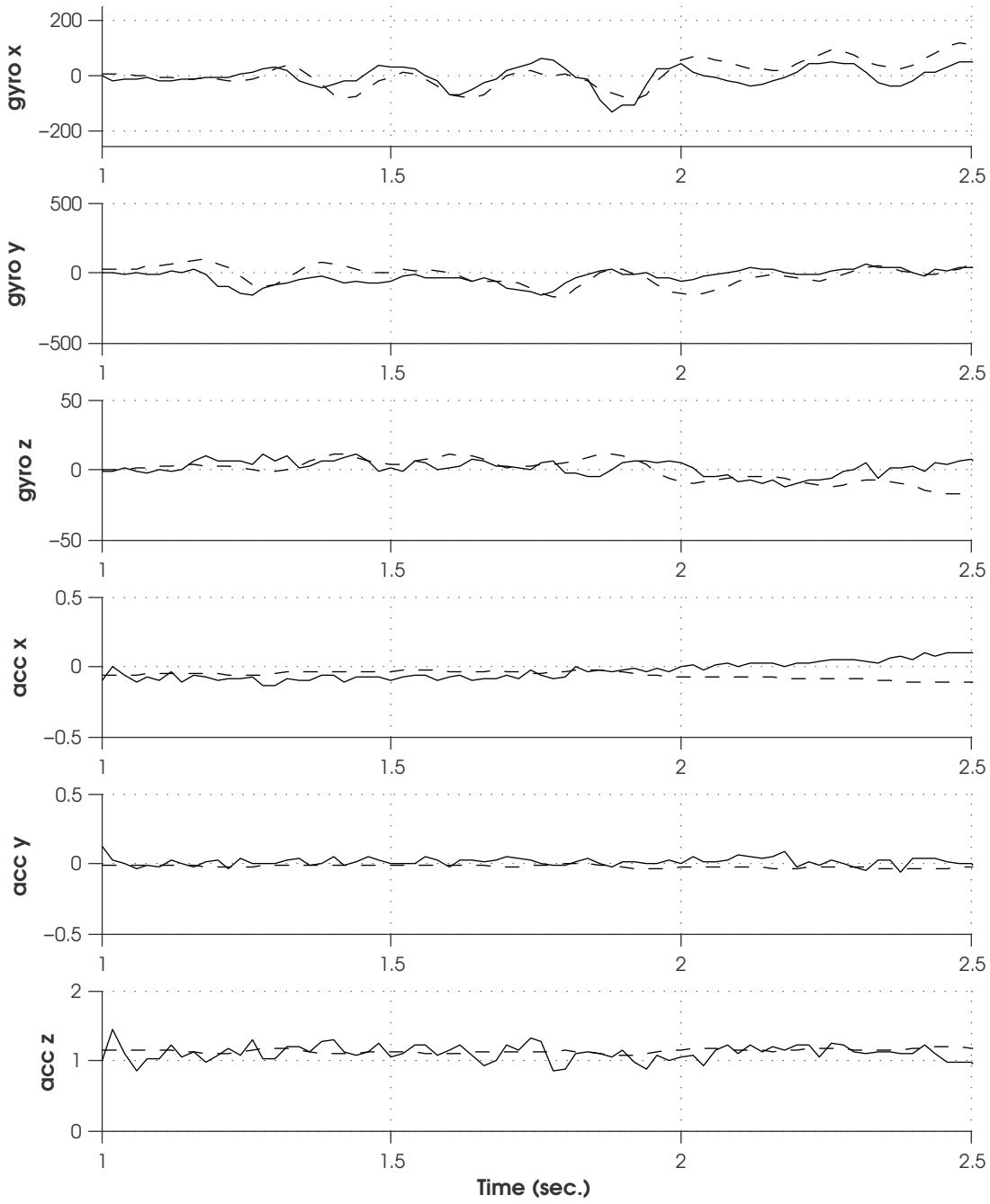

Figure 5.5: Simulated (dashed) response of identified model to pitch input compared with measured system response (solid).

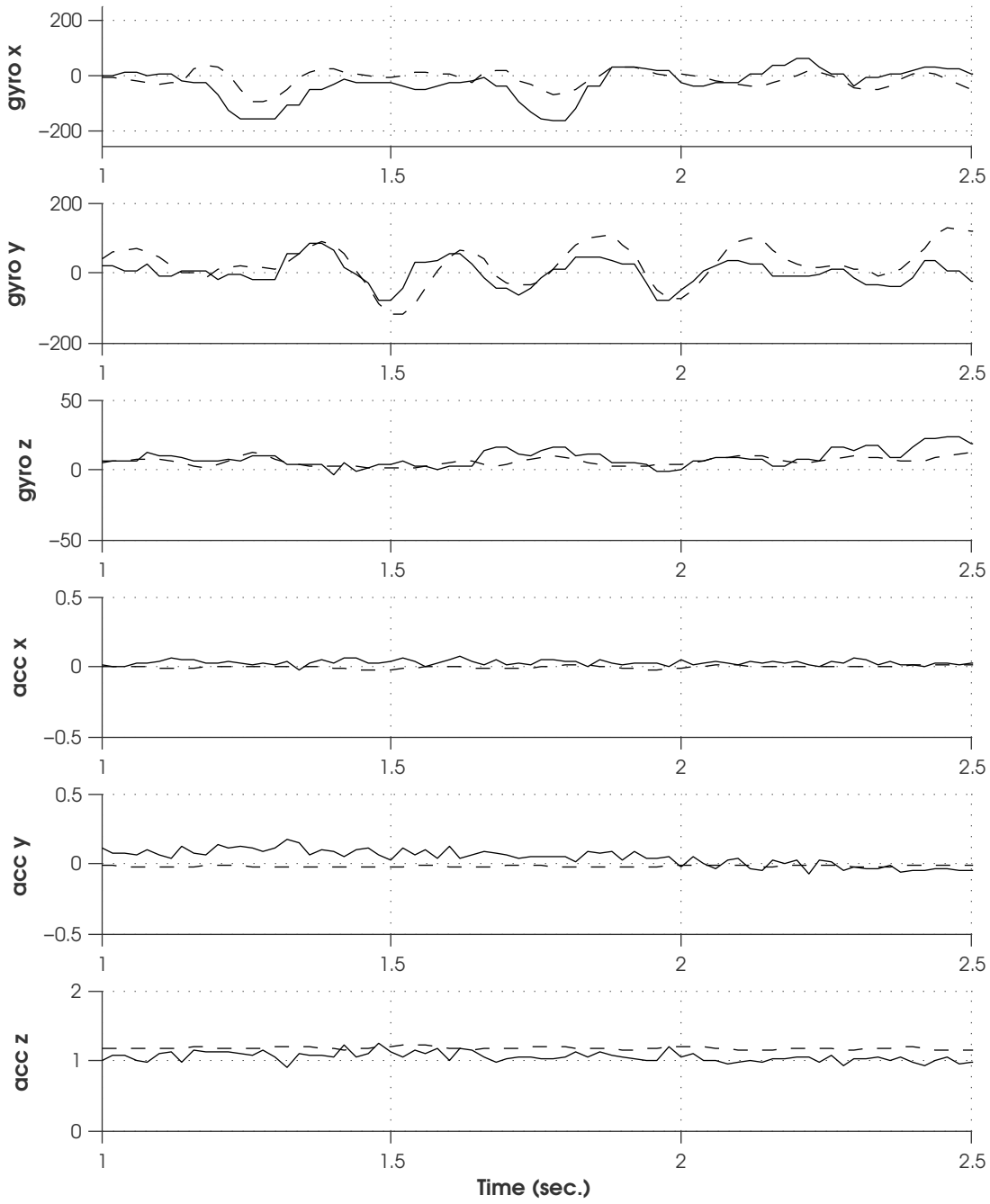

Figure 5.6: Simulated (dashed) response of identified model to roll input compared with measured system response (solid).

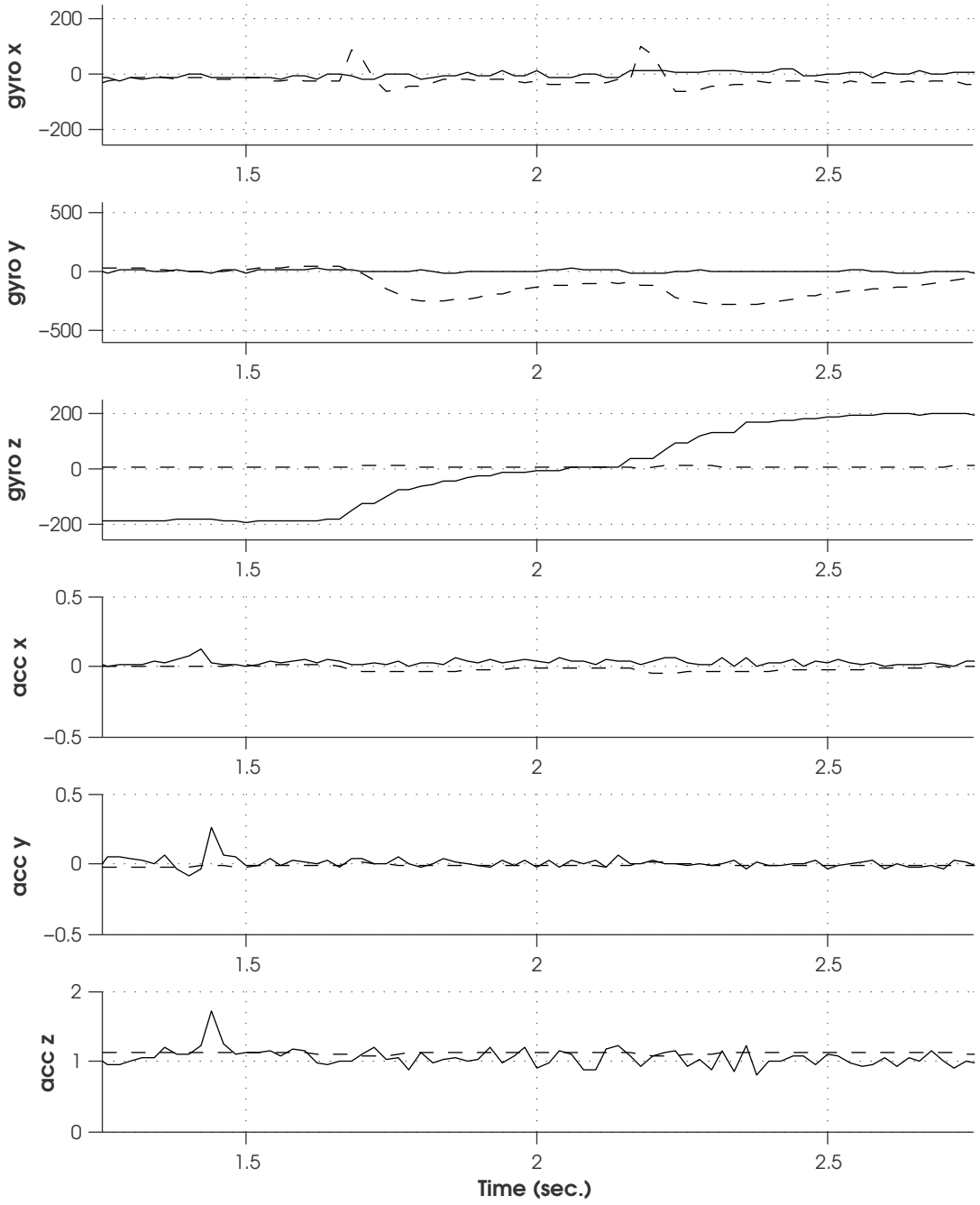

Figure 5.7: Simulated (dashed) response of identified model to yaw input compared with measured system response (solid).

5.3 Comparing Identified Model Performance From PO-MOESP and IEM Algorithms With Closed-Loop Data

In addition to evaluating the performance of a model identified using a closed loop subspace identification method (IEM), we analyzed the performance of a model identified from the same closed-loop data using a traditional subspace identification method which makes no attempt to correct (PO-MOESP). Because we used the same input-output data to develop both models, the only differences between the two models are due to the identification algorithms used.

Unlike IEM, the PO-MOESP algorithm assumes no correlation between system input an past noise (an invalid assumption in this case), with the effect of violating this assumption is easily seen in Figure 5.8. Because PO-MOESP makes no attempt to deal with the coupling between the input and noise terms however, the model identified using PO-MOESP does not suffer from the issue of having true system dynamics pre-estimated out. The result is that although the magnitudes of estimated system responses are incorrect, the model identified using PO-MOESP tracks the true system better than the IEM model in some cases. Despite this fact, the IEM model provides a more correct representation of the overall dynamics of the physical system in the presence of closed-loop data.

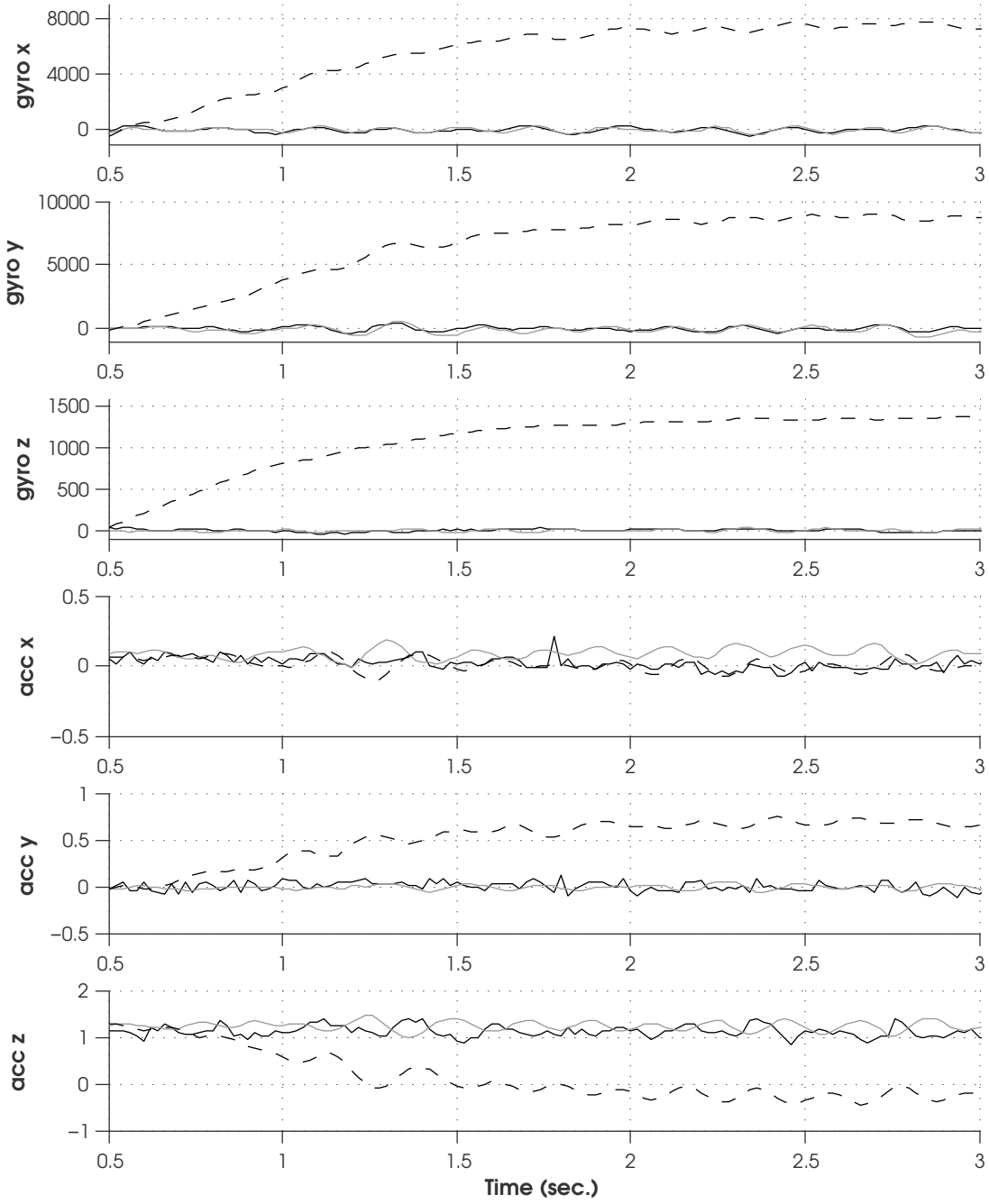

Figure 5.8: Simulated (dashed) response of identified model to yaw input compared with measured system response (solid). IEM results are plotted in light gray (solid) for reference.

CHAPTER 6

Conclusions and Future Work

The problem of black-box model identification of the dynamics of a quadro- tor helicopter has been considered. In view of the open-loop instability of the quadrotor, closed-loop experiments have been carried out and a continuous- time subspace model identification approach capable of dealing with such experimental conditions has been adopted. Furthermore, a complete anal- ysis of the uncertainty associated with the identified model has been per- formed, using tools from the field of computational statistics. The results of the study show that the considered approach is an effective one as far as the characterisation of the local dynamics of the quadrotor is concerned and can also provide useful uncertainty information for the purpose of robust con- trol system design, both in the frequency-domain and in the time-domain.

In this thesis a rigid-body simulator capable of simulating aircraft be- haviour has been developed and used to investigate the least squares method of system identification. Simulations confirms several methods for correcting sensor data for systematic errors. Wind vanes can be cor- rected for local winds caused by angular velocity and non-linear filters can estimate biases in gyro measurments under the conditions simulated. Non-linear observers have also been proposed to replace wind vanes and pitot-static tube, and simulations indicate that they might be useful for estimating the angle of attack, sideslip angle and dynamic pressure, pro- vided that there is no wind or gust during flying. This would simplify the instrumental setup and provide a faster and cheaper way of gathering data for

system identification. UAV control systems mighh already have the necessary hardware and logging capabilities to provide a useful data set for model building. Ordinary least squares method for identification of aircraft dynamics is not ideal since the solution is expected to be biased due to unlinearities even when assuming white sensor noise. Despite this, under the circumstances simulated biases are relative small and it can be argued that the results are useful. At least for initial estimation. Coeffi- cient of determination has been applied to explain how well the identified model is able to account for the variations of the measured data. Some issues concerning the validity of these coefficients when used on noisy data have been discussed.

As a result of the modeling, simulation, flight testing, and validation processes on a one-third scale Yak-54 platform documented in this thesis, the following conclusions can be made:

6.1 Conclusions

In comparison to approaches which individually identify decoupled system modes, we present results which identify a fully coupled 6DOF LTI system model.

6.2 Future Work

Based on the results presented as a result of this research,

investigate methods to optimize the selection of L and J in PARSIM E algorithm

(above is mine)

suggestions can be made to extend the scope of this research work. These suggestions are:

Optimize input sequences

Thus, it can be considered as future work to...

References

[1] Anil Ufuk Batmaz, Ovunc Elbir, and Cosku Kasnakoglu. Design of a quadrotor roll controller using system identification to improve empirical results. 2013.

[2] Bitcraze. http://www.bitcraze.se, 2013.

[3] Anthony RS Bramwell, David Balmford, and George Done. *Bramwell's helicopter dynamics*. Butterworth-Heinemann, 2001.

[4] Tommaso Bresciani. *Modelling, identification and control of a quadrotor helicopter*. Department of Automatic Control, Lund University, 2008.

[5] Caleb Chamberlain. System identification, state estimation, and control of unmanned aerial robots. Master's thesis, Brigham Young University, 2011.

[6] Alessandro Chiuso and Giorgio Picci. Consistency analysis of some closed-loop subspace identification methods. *Automatica*, 41(3):377–391, 2005.

[7] Jorge Miguel Brito Domingues. Quadrotor prototype. *Instituto Superior Tecnico*, 2009.

[8] Gene F. Franklin, Powell J. David, and Michael Workman. *Digital Control of Physical Systems*. Addison-Wesley, third edition, 1998.

[9] Shweta Gupte, Paul Infant Teenu Mohandas, and James M Conrad. A survey of quadrotor unmanned aerial vehicles. In *Southeastcon, 2012 Proceedings of IEEE*, pages 1–6. IEEE, 2012.

[10] Gabriel M Hoffmann, Haomiao Huang, Steven L Waslander, and Claire J Tomlin. Quadrotor helicopter flight dynamics and control: Theory and experiment. In *Proc. of the AIAA Guidance, Navigation, and Control Conference*, pages 1–20, 2007.

[11] Magnus Jansson. On subspace methods in system identification and sensor array signal processing. *These de doctorat-Royal institute of technology, Stockholm*, 1997.

[12] Rudolph Emil Kalman et al. A new approach to linear filtering and prediction problems. *Journal of basic Engineering*, 82(1):35–45, 1960.

[13] Tohru Katayama. *Subspace methods for system identification*. Springer, 2005.

[14] László Kis and Béla Lantos. Sensor fusion and actuator system of a quadrotor helicopter. *Electrical Engineering and Computer Science*, 53(3-4):139–150, 2011.

[15] Arda Özgür Kivrak. Design of control systems for a quadrotor flight vehicle equipped with inertial sensors. *Atilim University, December*, 2006.

[16] Wallace E Larimore. Canonical variate analysis in identification, filtering, and adaptive control. In *Decision and Control, 1990., Proceedings of the 29th IEEE Conference on*, pages 596–604. IEEE, 1990.

[17] Gigun Lee, Dong Yun Jeong, Nguyen Dang Khoi, and Taesam Kang. Attitude control system design for a quadrotor flying robot. In *Ubiquitous Robots and Ambient Intelligence (URAI), 2011 8th International Conference on*, pages 74–78. IEEE, 2011.

[18] Daniel Mellinger, Michael Shomin, and Vijay Kumar. Control of quadrotors for robust perching and landing. In *Proc. Int. Powered Lift Conf*, pages 119–126, 2010.

[19] Bernard Mettler, Takeo Kanade, and Mark Brian Tischler. *System identification modeling of a model-scale helicopter*. Carnegie Mellon University, The Robotics Institute, 2000.

[20] Nathan Michael, Daniel Mellinger, Quentin Lindsey, and Vijay Kumar. The grasp multiple micro-uav testbed. *Robotics & Automation Magazine, IEEE*, 17(3):56–65, 2010.

[21] Derek Miller. *Open Loop System Identificaiton of a Micro Quadrotor Helicopter from Closed Loop Data*. PhD thesis, 2011.

[22] Paul Pounds, Robert Mahony, and Peter Corke. Modelling and control of a quad-rotor robot. In *Proceedings Australasian Conference on Robotics and Automation 2006*. Australian Robotics and Automation Association Inc., 2006.

[23] S Joe Qin. An overview of subspace identification. *Computers & chemical engineering*, 30(10):1502–1513, 2006.

[24] S Joe Qin and Lennart Ljung. Closed-loop subspace identification with innovation estimation. In *Proceedings of SYSID*, volume 2003, 2003.

[25] Zak Sarris and STN ATLAS. Survey of uav applications in civil markets (june 2001). In *The 9 th IEEE Mediterranean Conference on Control and Automation (MED'01)*, 2001.

[26] Matthias Schreier. Modeling and adaptive control of a quadrotor. In *Mechatronics and Automation (ICMA), 2012 International Conference on*, pages 383–390. IEEE, 2012.

[27] Torsten Söderström and Petre Stoica. *Instrumental variable methods for system identification*, volume 161. Springer-Verlag Berlin, 1983.

[28] Pavel Trnka. *Subspace identification methods*. PhD thesis, Ph. D. dissertation, Czech Technical University in Prague, 2007.

[29] Kimon P Valavanis. *Advances in unmanned aerial vehicles: state of the art and the road to autonomy*, volume 33. Springer, 2007.

[30] Gijs van der Veen, Jan-Willem van Wingerden, Marco Bergamasco, Marco Lovera, and Michel Verhaegen. Closed-loop subspace identification methods: an overview. *IET Control Theory & Applications*, 7(10):1339–1358, 2013.

[31] Peter Van Overschee and Bart De Moor. N4sid: Subspace algorithms for the identification of combined deterministic-stochastic systems. *Automatica*, 30(1):75–93, 1994.

[32] Peter Van Overschee and Bart De Moor. A unifying theorem for three subspace system identification algorithms. *Automatica*, 31(12):1853–1864, 1995.

[33] Michel Verhaegen. Identification of the deterministic part of mimo state space models given in innovations form from input-output data. *Automatica*, 30(1):61–74, 1994.

[34] Michel Verhaegen and Patrick Dewilde. Subspace model identification part 1. the output-error state-space model identification class of algorithms. *International journal of control*, 56(5):1187–1210, 1992.

[35] Michel Verhaegen and Vincent Verdult. *Filtering and system identification: a least squares approach*. Cambridge university press, 2007.

[36] Mats Viberg. Subspace-based methods for the identification of linear time-invariant systems. *Automatica*, 31(12):1835–1851, 1995.

[37] Stacy S Wilson. Understanding the prbs signal as an optimum input signal in the wavelet-correlation method of system identification using multiresolution analysis. In *SoutheastCon, 2005. Proceedings. IEEE*, pages 39–44. IEEE, 2005.